Pergamon

Geochimica et Cosmochimica Acta, Vol. 65, No. 12, pp. 1933–1951, 2001

0016-7037/01 $20.00 + .00

PII S0016-7037(00)00545-2

Solubility of copper in silicate melts as function of oxygen and sulfur fugacities, temperature, and silicate composition

A. HOLZHEID[1,2,†] and K. LODDERS[2,*]

[1]Institut für Mineralogie und Geochemie, Universität zu Köln, Zülpicher Straβe 49b, 50674 Köln, Germany
[2]Planetary Chemistry Laboratory, Department of Earth and Planetary Sciences and McDonnell Center for the Space Sciences, Washington University, Campus Box 1169, One Brookings Drive, St. Louis, MO 63130-4899, USA

(*Received July* 27, 2000; *accepted in revised form November* 10, 2000)

Abstract—The solubility of Cu in silicate melts coexisting with liquid Cu(Fe) metal and liquid Cu(Fe) sulfide was determined experimentally at oxygen fugacities ranging from $10^{-9.1}$ to $10^{-13.6}$ bar and sulfur fugacities ranging from $10^{-2.5}$ to $10^{-6.3}$ bar at 1300°C. An iron oxide-free silicate of anorthite-diopside eutectic composition and a synthetic MgO-rich basaltic silicate (FeO-bearing) were used in the partitioning experiments. In S-containing systems, some of the metal reacted to metal sulfide. The silicates in the four systems investigated (Fe-free and S-free; Fe-containing and S-free; Fe-free and S-containing; Fe-containing and S-containing) had different colors depending on the dissolved Cu species and the presence of iron and/or sulfur.

Irrespective of the presence of sulfur, the solubility of Cu in the silicate increases with increasing oxygen fugacity and metal/silicate partition coefficients for Cu decrease. Increasing the temperature from 1300°C to 1514°C increases the Cu solubility (decreases the metal/silicate partition coefficient) at an oxygen fugacity 0.5 log units below the iron–wüstite (IW) equilibrium in the Fe-free, S-free and Fe-containing, S-free systems. We infer the presence of monovalent Cu^+ ("$CuO_{0.5}$") in the silicate melt on the basis of the solubility of Cu as function of oxygen fugacity. Experiments containing iron yield a formal valence of ~0.5 for Cu at very low oxygen fugacities, which is not observed in Fe-free systems. The low formal valence is explained by redox reactions between iron and copper in the silicate melts.

There is no evidence for sulfidic dissolution of Cu in the silicates but sulfur has indirect effects on Cu partitioning. Iron metal/silicate partition coefficients depend on oxygen fugacity and on sulfur fugacity. Sulfidic dissolution of iron and oxide-sulfide exchange reactions with Cu cause a small increase in Cu metal/silicate partition coefficients.

We derive an activity coefficient ($\gamma_{CuO_{0.5}}$) of 10 ± 1 for liquid $CuO_{0.5}$ at 1300°C for the silicate melts used here. A comparison with literature data shows that log $\gamma_{CuO_{0.5}}$ increases in proportion to the mass percentages $[CaO + (Al_2O_3)/2]$ in silicate melts.

We recommend the following equations for Cu metal/silicate and sulfide/silicate partitioning for geochemical and cosmochemical modeling if silicate composition and the activity of Cu in the metal or sulfide is known:

$$\log D^{met/sil} = -0.48 - 0.25 \cdot \log fO_2 - \log \gamma_{Cu_{metal}} + 0.02 \cdot [CaO + (Al_2O_3)/2; wt\%]_{silicate}$$

$$\log D^{sul/sil} = +0.76 - 0.25 \cdot \log fO_2 + 0.25 \log fS_2 - \log \gamma_{CS_{0.5},sulfide} + 0.02 \cdot [CaO + Al_2O_3/2; wt\%]_{silicate}.$$

The derived Cu metal/silicate and metal/sulfide partition coefficients are applied to core formation in the Earth and Mars. The observed Cu abundances in the Earth cannot be easily explained by simple core-mantle equilibrium, but the observed Cu abundances for Mars are consistent with core-mantle equilibrium at low pressure and temperatures.

1. INTRODUCTION

Knowledge about the partitioning of elements between metal, sulfide, and silicate phases is required for understanding differentiation processes in the Earth and other planetary bodies. Formation of a metal or metal sulfide protocore in a planet will remove siderophile (metal-seeking, e.g., Fe, Ni, Co, noble metals) and/or chalcophile (sulfide-seeking, e.g., Cu, Pb, Zn) elements from the silicate protomantle into the separating metallic phase. Absolute and relative abundances of siderophile and chalcophile elements in the silicate mantle after cessation of core formation provide information about the type and extent of the core formation process, when compared with calculated abundances from experimentally determined metal/silicate and sulfide/silicate partition coefficients.

There are many studies in the metallurgical literature on the solubility of Cu in silicate melts, mainly iron silicate (fayalitic) slags (e.g., Ruddle et al., 1966; Toguri and Sandanter, 1969, 1972; Altman and Kellogg, 1972; Nagamori, 1974; Altman, 1978; Elliot et al., 1978; Reddy and Acholonu, 1984). More recently, Ripley and Brophy (1995) studied the solubility of Cu in sulfur-free mafic melts. All these studies have the presence of pure Cu metal or Cu-rich metal alloys in common. The only study that used Cu in trace amounts for experimental Cu partitioning between basaltic silicate and Fe-rich metal is by Schmitt et al. (1989). All studies show that the solubility of Cu in silicate decreases with de-

*Author to whom correspondence should be addressed (lodders@levee.wustl.edu).
†*Present address:* Institut für Minerologie Westfälische Wilhelms–Universität Münster. Corrensstraße 24 48149 Münster, Germany (holzheid@hwz.uni-muenster.de).

Table 1. Silicate starting compositions.[a]

Concentration, wt%	AD	BK
SiO_2	50.88 (0.7)	49.05 (0.5)
Al_2O_3	13.75 (1)	14.07 (0.9)
MgO	10.36 (0.8)	10.61 (0.9)
CaO	24.89 (0.6)	19.24 (0.3)
FeO	0	6.95 (0.9)
total	99.88	99.92

[a] Electron microprobe analysis. Numbers in parentheses are 1σ deviations in percentages. AD, anorthite–diopside eutectic mixture; BK, MgO-rich basalt.

creasing oxygen fugacity. The solubility of Cu is also affected by silicate composition; see, e.g., Ruddle et al. (1966), Altman (1978), Elliot et al. (1978), and Reddy and Acholonu (1984).

Sulfide/silicate partitioning of Cu was investigated experimentally by, e.g., Ruddle et al. (1966), Nagamori (1974), and Rajamani and Naldrett (1978), but these studies do not include a metal phase. A few determinations of (metal + sulfide)/silicate partition coefficients for Cu present in trace amounts by Lodders and Palme (1991) show an increase of Cu concentrations in iron sulfide with increasing S content of the Fe sulfide, implying that Cu is more chalcophile than siderophile.

In this article, we systematically investigate the partitioning of Cu between metal, sulfide, and silicate as function of oxygen and sulfur fugacities, temperature, and silicate composition.

2. MATERIALS AND METHODS

Silicate liquids were equilibrated with liquid Cu (melting point 1083°C) and liquid CuFe alloys. Silicate starting material was either an anorthite–diopside silicate powder (FeO-free) or a MgO-rich basaltic silicate (FeO-bearing). The compositions of both silicates are given in Table 1. Both starting silicates were prepared by mixing of reagent-grade oxide powders that were melted in corundum crucibles in air, quenched to glass, and then ground to a powder. Commercial Cu powder (<22 mesh, purity: 99.999%, Alfa Chemicals) was used.

Mixtures of silicate and pure metal powder (500–750 mg total; 60 wt% silicate, 40 wt% metal) were transferred into small corundum crucibles (6 mm in diameter) and equilibrated in Deltech vertical tube furnaces at 1 atm under different oxygen and sulfur fugacities, and temperatures at the Planetary Chemistry Laboratory, Washington University, St. Louis. Up to six corundum crucibles per experiment were simultaneously placed in the isothermal hot zone of the furnace. Identical run numbers in Table 2 identify samples that were heated simultaneously. Run durations varied between 5.5 and 75 h. Three types of experiments were performed: (1) under controlled oxygen fugacities (S-free system), (2) under constant oxygen fugacity but varying sulfur fugacities, and (3) under varying oxygen fugacities but constant sulfur fugacity. CO-CO_2 gas mixtures controlled the oxygen fugacities in S-free systems. Oxygen and sulfur fugacities in the S-bearing experiments were controlled by CO-CO_2-SO_2 gas mixtures. The temperature and oxygen fugacity were measured with a $PtRh_6/PtRh_{30}$ thermocouple and a CaO-Y_2O_3–stabilized ZrO_2 solid electrolyte sensor, respectively. The sulfur fugacity was (a) calculated from the chemical equilibrium composition of the CO-CO_2-SO_2 gas mixtures that used the thermodynamic properties of the coexisting gases (Gurvich et al., 1989; Chase, 1998), and (b) determined after the experiment from the stoichiometry of iron sulfide, which was placed in the furnace together with the other samples. The Fe/S ratio of pyrrhotite is a function of fS_2 and can be used to check the prevailing fS_2 during the experiments. The analytical method to determine the sulfur fugacity will be described in more detail in the future.

Samples were quenched by withdrawing the charge rapidly from the hot zone to the cooler top of the furnace. Silicate glass and metal (−sulfide) was separated by crushing the sample-containing corundum crucible and by handpicking of individual glass and metal (+sulfide) fragments. Aliquots of silicate, metal, and metal sulfide phases were mounted in epoxy and polished for microprobe analysis. Silicates, metal, and metal sulfide phases of S-containing runs were analyzed by electron microprobe (EMP) with a JEOL-733 superprobe at Washington University, St. Louis. Silicate and metal phase compositions of S-free experiments were determined by a Cameca SX 50 microprobe at Bayerisches Geoinstitut, Bayreuth. Beam currents of 30 nA (Jeol 733) and 15 nÅ (Cameca SX 50), an accelerating voltage of 15 kV (Jeol 733, Cameca SX 50) and counting times between 20 and 60 s, depending on expected concentration levels in silicate, metal, and metal sulfide phases, were employed. Possible matrix effects were corrected by the ZAF routine for Jeol 733 analyses (e.g., Armstrong, 1988) and PAP routine for Cameca SX 50 analyses (e.g., Pouchou and Pichoir, 1984).

Attainment of equilibrium between silicate, metal, and metal sulfide phases was demonstrated by homogeneous distribution of the elements in the three individual phases and by time series experiments of S-containing systems with anorthite–diopside silicates with run durations between 5 and 68 h (S-I-22, S-I-23, S-I-24, and S-I-25; Table 2). Diffusion length scales of 0.5 cm/h derived from the diffusion coefficient of Cu at 1300°C in fayalitic melts (Ajersch and Toguri, 1969) indicate that run durations here should be sufficient to allow sample equilibration. Experiments done for more than 10 h appear texturally and compositionally homogeneous and equilibrated, consistent with run durations reported in the literature for much larger sample sizes (e.g., Toguri and Santander, 1969; Elliot et al., 1978). Schreiber et al. (1992) showed that run times of 4 h are sufficient for equilibrating small samples for amber coloring with SO_2-containing gases. Samples that have inhomogeneous coloring and compositions were excluded from our numerical data analyses.

3. RESULTS

We first describe the microstructures of the run products and the results of the electron microprobe measurements of the coexisting phases. Experimental parameters (temperature, oxygen and sulfur fugacities, and run duration) and the results of the electron microprobe analyses of silicate, metal sulfide, and alloy phases for each experiment are summarized in Table 2. The different systems (Fe-free, S-free; Fe-bearing, S-free; Fe-free, S-bearing; Fe-bearing, S-bearing) are distinguished by use of the notation (−Fe, −S), (+Fe, −S), (−Fe, +S), and (+Fe, +S) where "+" means that the element is present in the system and "−" indicates its absence.

3.1. Phase Assemblages and Compositions

The silicate–sulfide–metal assemblages show clear separation of metal and sulfide from the silicate glass after the experiment, independent of the Fe and S content in the coexisting phases. At run temperatures 200°C above the melting point of pure Cu metal (mp. 1083°C) formation of molten Cu droplets occurs in the silicate. These Cu droplets agglomerated into one big Cu sphere that settled down to the bottom of the alumina crucible when sulfur was absent. When sulfur was present in the charge, Cu metal and Cu or (CuFe) sulfide were concentrated at the top of the silicate liquid. Typically a sulfide rim formed around Cu metal. Figure 1 shows a reflected light micrograph of Cu metal (bright phase) surrounded by Cu sulfide (darker rim) from experiment ADCu S-II-7 (−Fe, +S). Despite the sharp boundary between the Cu sulfide and Cu metal, sulfide droplets are present in the Cu sphere and Cu droplets are present in the sulfide rim. This is found in all charges. Therefore, we can assume that the surrounding silicate liquid phase was in direct contact with Cu (or CuFe) metal and

Table 2. Experimental parameters and phase compositions.[a]

Run	T, °C	t, h	log fO_2	ΔIW	log fS_2	Metal Cu	Metal Fe	Metal S	Sulfide Cu	Sulfide Fe	Sulfide S	Silicate SiO_2	Silicate MgO	Silicate Al_2O_3	Silicate CaO	Silicate FeO	Silicate Cu	Silicate S	Total
Fe-free, S-free system (−Fe, −S)																			
C-C-1	1302	46.6	−9.19	+1.53		100						50.4 (0.8)	9.84 (0.8)	15.9 (0.6)	23.1 (0.9)		0.327 (12)		99.7
C-C-9	1300	62.0	−10.66	+0.09		100						50.5 (0.4)	9.60 (0.6)	16.0 (0.5)	23.2 (0.9)		0.185 (20)		99.5
C-C-4	1302	45.9	−11.34	−0.62		100						50.1 (0.4)	9.79 (1)	16.3 (0.6)	23.0 (0.9)		0.109 (17)		99.3
C-C-3	1303	45.8	−12.43	−1.71		100						50.6 (0.6)	9.74 (0.8)	16.1 (0.4)	22.9 (0.9)		0.041 (29)		99.4
C-C-2	1304	46.5	−13.55	−2.85		100						50.4 (0.8)	10.1 (1)	15.5 (1)	23.1 (0.4)		0.036 (22)		99.1
C-C-6	1407	21.1	−10.20	−0.56		100						46.4 (0.6)	8.69 (0.9)	22.9 (0.4)	21.0 (0.4)		0.136 (14)		99.3
C-C-8	1459	30.1	−9.66	−0.50		100						41.5 (2)	4.23 (62)	33.8 (4)	19.3 (2)		0.162 (45)		99.0
C-C-7	1514	9.0	−9.10	−0.43		100						39.3 (0.8)	6.06 (1)	35.0 (0.6)	17.9 (0.6)		0.250 (12)		98.6
Fe-bearing, S-free system (+Fe, −S)																			
C-C-1	1302	46.6	−9.19	+1.53		98.2 (8)	0.07 (86)					48.4 (0.6)	9.48 (0.7)	15.7 (1)	22.6 (0.4)	2.80 (3)	0.355 (10)		99.4
C-C-9	1300	62.0	−10.66	+0.09		95.1 (9)	3.23 (2)					47.3 (0.6)	10.0 (0.6)	16.0 (0.6)	20.1 (0.5)	5.92 (3)	0.159 (19)		99.5
C-C-4	1302	45.9	−11.34	−0.62		97.1 (8)	3.92 (2)					48.0 (0.6)	9.97 (0.5)	16.1 (0.6)	22.5 (0.4)	2.70 (4)	0.098 (48)		99.4
C-C-3	1303	45.8	−12.43	−1.71		97.4 (9)	1.13 (9)					48.2 (0.2)	10.1 (0.7)	16.0 (0.6)	22.6 (0.4)	2.42 (4)	0.077 (31)		99.4
C-C-2	1304	46.5	−13.55	−2.85		96.4 (10)	2.05 (15)					48.0 (0.6)	10.7 (0.6)	16.3 (1)	22.2 (0.5)	1.98 (3)	0.053 (26)		99.3
C-C-6	1407	21.1	−10.20	−0.56		97.1 (9)	2.50 (2)					42.2 (0.5)	8.10 (11)	26.5 (1)	19.7 (1)	2.49 (6)	0.116 (33)		99.1
C-C-7	1514	9.0	−9.10	−0.43		94.0 (10)	3.35 (1)					40.6 (0.5)	5.60 (0.7)	33.9 (9)	17.4 (0.5)	1.91 (5)	0.256 (18)		99.8
Fe-free, S-bearing system (−Fe, +S)																			
S-II-5	1301	73	−9.52	−1.22	−4.22	99.6 (10)		<0.01	79.7 (1)		20.3 (1)	49.1 (1)	8.29 (1)	16.3 (1)	24.0 (0.1)		0.337 (8)	<0.012	98.2
S-I-2	1300	8.3	−11.71	−0.96	−2.84	100 (1)		<0.01	79.8 (1)		19.8 (2)	50.6 (0.4)	9.24 (0.9)	15.3 (1)	24.5 (0.2)		0.126 (13)	<0.004	99.7
S-I-18	1300	71	−11.72	−0.97	−5.27	98.9 (10)		<0.35	79.5 (1)		20.1 (1)	50.2 (0.4)	8.66 (0.6)	16.6 (0.4)	24.5 (0.8)		0.116 (100)	n.d.[c]	100.1
S-I-23	1304	5.5	−11.75	−1.05	−6.29	—[b]		—[b]	—[b]		—[b]	50.0 (0.6)	9.02 (0.8)	15.1 (0.7)	23.9 (0.8)		0.097 (19)	0.012 (33)	98.1
S-I-25	1304	45	−11.78	−1.08	−6.29	100 (1)		0.02 (1)	80.2 (1)		20.0 (10)	49.7 (0.4)	8.50 (2)	16.5 (4)	23.9 (0.1)		0.089 (10)	0.016 (25)	98.7
S-I-22	1300	68	−11.83	−1.08	−6.29	100 (1)		0.02 (1)	80.6 (1)		19.6 (3)	50.5 (0.6)	8.75 (0.9)	16.6 (0.2)	24.6 (0.1)		0.089 (10)	<0.004	100.5
S-I-24	1305	18	−11.91	−1.22	−6.29	—[b]		—[b]	—[b]		—[b]	49.6 (0.1)	8.77 (1)	15.6 (1)	24.3 (0.1)		0.106 (10)	0.020 (20)	98.4
S-II-7	1300	31	−12.18	−1.43	−4.36	100 (1)		<0.10	79.9 (1)		18.7 (3)	49.3 (1)	8.56 (2)	15.8 (0.3)	24.5 (0.2)		0.071 (10)	0.016 (25)	98.3
S-II-8	1304	42	−12.63	−1.93	−4.36	100 (1)		<0.05	79.6 (1)		18.9 (3)	49.3 (0.1)	8.73 (0.7)	15.8 (0.5)	24.5 (0.4)		0.054 (9)	0.024 (17)	98.4
Fe-bearing, S-bearing system (+Fe, +S)																			
S-II-5	1301	73	−9.52	−1.22	−4.22	100 (1)	0.06 (33)	<0.01	79.6 (1)	0.54 (41)	20.1 (7)	46.7 (0.4)	9.51 (0.8)	17.5 (1)	17.8 (0.3)	6.30 (4)	0.208 (8)	0.012 (33)	98.1
S-I-2	1300	8.3	−11.71	−0.96	−2.84	100 (1)	0.48 (19)	0.13	76.8 (1)	2.07 (9)	21.2 (0.9)	49.0 (0.2)	10.7 (0.9)	14.3 (0.7)	18.6 (0.4)	6.30 (0.3)	0.080 (11)	<0.008	99.0
S-I-18	1300	71	−11.72	−0.97	−5.27	97.7 (10)	1.07 (0.9)	0.15	74.8 (1)	3.44 (12)	22.1 (0.9)	48.3 (0.2)	9.82 (0.7)	17.5 (0.6)	18.4 (1)	5.83 (0.3)	0.072 (36)	<0.008	100.0
S-I-14	1301	65	−11.74	−1.00	−4.22	99.5 (40)	0.44 (70)	<0.01	70.7 (1)	6.12 (2)	22.8 (0.9)	48.8 (0.6)	10.1 (1)	17.4 (0.1)	18.7 (0.2)	5.18 (1)	0.112 (63)	0.016 (25)	100.2
S-I-22	1300	68	−11.83	−1.08	−6.29	98.0 (10)	1.71 (4)	<0.01	72.1 (1)	5.54 (3)	22.9 (0.9)	48.2 (0.4)	10.1 (0.4)	17.1 (0.1)	18.6 (0.1)	6.13 (0.5)	0.080 (11)	n.d.	100.2
S-I-5	1303	8.6	−11.86	−1.15	−2.50	100 (1)	0.17 (12)	<0.01	73.3 (1)	5.25 (5)	22.6 (0.9)	51.0 (0.4)	11.1 (0.1)	16.3 (0.4)	19.3 (0.3)	2.54 (0.4)	0.044 (20)	0.036 (11)	100.3
S-II-7	1300	31	−12.18	−1.43	−4.36	—[d]	—[d]	—[d]	74.6 (0.9)	4.30 (11)	22.2 (2)	47.5 (1)	9.85 (3)	16.5 (0.1)	18.5 (0.3)	5.30 (0.2)	0.056 (11)	0.032 (38)	97.8
S-II-9	1303	69	−12.47	−1.76	−4.61	100 (1)	0.69 (32)	<0.01	71.9 (2)	5.42 (21)	21.8 (5)	48.8 (1)	10.1 (0.3)	17.1 (0.1)	19.0 (0.1)	3.42 (0.3)	0.080 (45)	0.024 (33)	98.5

[a] All concentrations are given in wt%, as determined by electron microprobe analyses. Numbers in parentheses are 1σ deviations in percentages. The oxygen fugacity (fO_2) is from zirconia oxygen-sensor measurements. The sulfur fugacity (fS_2) is calculated from CO_2-CO-SO_2 equilibria.

[b] Metal and sulfide phases were lost during sample preparation.

[c] n.d., not detected.

[d] Metal phase absent in section.

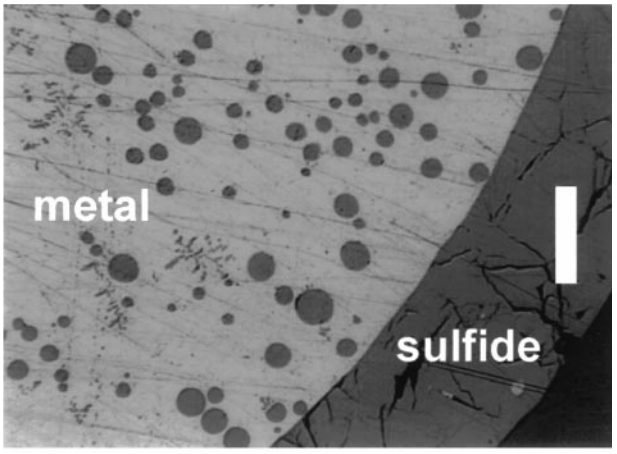

Fig. 1. A reflected light microscopy picture of Cu metal (bright) surrounded by Cu sulfide (dark) of experiment ADCu S-II-7. Despite the sharp boundary between the Cu sulfide and the Cu metal, Cu_2S droplets are present in the Cu sphere and Cu droplets are present in the Cu_2S rim. Magnification, 10×; vertical scale bar = 160 μm.

Cu (or CuFe) sulfide. The spherical shape of metal droplets in the sulfide rim and sulfide droplets in the metal sphere reflect the coexistence of liquid metal and liquid sulfide during the experiment. Typical dentritic S-rich exsolution textures in the metal (visible in the upper left-hand corner of Fig. 1) were likely formed during quenching.

In Fe-containing runs, homogeneous CuFe alloys with up to 4 wt% Fe formed, depending on the oxygen fugacity prevailing during the experiment. In S-containing experiments, a Cu or CuFe sulfide formed around the Cu- or CuFe alloy spheres. The S-content (~20 wt%) of the Cu sulfides indicates stoichiometric Cu_2S, in accordance with the Cu-S phase diagram. The presence of Cu_2S was verified by X-ray diffraction (XRD). The sulfides in the Fe-bearing experiments are pseudobinary solutions of Cu_2S and FeS. Sulfur was homogeneously distributed within the sulfides, regardless of the Fe content (0.5–6.1 wt%) in the CuFe sulfides.

The silicate composition in all charges was homogeneous in major and minor elements, including Cu and S. The absolute Cu content of the silicate glass depends strongly on the oxygen fugacity and ranges between ~350 and 3400 ppm with slightly higher Cu concentrations in Fe-free charges. Depending on the sulfur fugacity, the S content of the silicate glass in Fe-free and Fe-bearing charges ranged from 40 to 240 ppm. No significant difference was found in the S content of Fe-free and Fe-bearing silicates. The initial FeO content of the Fe-bearing silicate (7 wt% FeO) decreased by a factor of 1.5 to 2.5 because of formation of CuFe alloys (in S-free charges) and additional CuFe sulfides (in S-containing charges) during the experiments. The resulting Fe content in the alloys and sulfides were up to 1.7 and 6 wt%, respectively.

3.2. Colors

The silicates resulting from the experiments show a variety of colors. It is known from glass coloring studies (e.g., Weyl, 1954) that colors of silicate glasses can provide clues about the valences of the dissolved species present. We use the observed colors of the silicates as a guide in the interpretation of valences below. The silicate colors of the four different systems are described briefly next and summarized in Table 3. These silicate colors are assigned to the symbols used to plot the partition coefficients in Figure 2.

The silicates in the iron and sulfur-free systems (−Fe, −S) are colorless, clear, and transparent. With decreasing fO_2, a slight grayish discoloration becomes visible, which is known to occur during the formation of copper-ruby glass (Dietzel, 1945).

The glasses in the Fe-free and sulfur-containing system (−Fe, +S) are transparent and clear. The silicate from the run at the highest fO_2 is colorless. The experiment S-I-2 was done at the highest fS_2 and yielded a pale green glass. With decreasing oxygen fugacity, the silicates become slightly reddish, which is probably due to suspended metallic Cu (copper-ruby). According to Weyl (1954) and Richardson and Billington (1956), copper-ruby forms when fine colloidal metal Cu is present in the silicate during melting, and upon quenching, the silicate glass remains supersaturated in metallic copper (typically <1%). However, only very small amounts of colloidal Cu are needed to create the coloration. The Cu content in the Fe-free silicates is somewhat higher when sulfur is present so that more colloidal metallic Cu may intensify the coloration in the silicates of the (−Fe, +S) experiments. The reddish tint is restricted to experiments with low sulfur fugacities. At low fO_2 and sulfur fugacities of about log $fS_2 = -4.4$, the silicates are honey yellow to yellow brown. The color could be related to small amounts of dissolved sulfur in the form of polysulfides, which is the cause of glass amber coloring, according to Schreiber et al. (1992). These authors explain that amber coloring occurs when metal cations with suitable redox potentials allow the oxidation of S^{2-} to the supersulfide ion $(S_2)^-$. At the lowest oxygen fugacities here, the pair Cu^0-Cu^+ appears to have the appropriate redox potential to produce the yellow color. It is unlikely that the coloring is due to the presence of Cu_2S because the solubility of copper sulfide in glass is extremely low and copper sulfide exsolves easily from silicate melt (Weyl, 1954).

The glasses in the Fe-bearing and S-free system (+Fe, −S) are all transparent and clear. At the highest oxygen fugacities, the silicates are deep, dark green-bluish and medium green at the next lowest fO_2. The three experiments at the lowest fO_2 are intensive turquoise and slightly bluish, with the intensity decreasing toward lower fO_2.

The silicates from the Fe- and S-bearing system (+Fe, +S) are deeply colored. The runs at the highest fS_2 ($\sim 10^{-2.5}$) yielded green glasses. Run S-I-2 in this series was inhomogeneously brown/green, and therefore we did not use that experiment in our data analyses below. The other run at this fS_2 appears to be equilibrated and is of dark green color. The experiments at $fS_2 \sim 10^{-4.4}$ are all red-brown opaque, irrespective of the fO_2, which ranges from $fO_2 = 10^{-9.5}$ to $10^{-12.5}$ in this set. Experiments at the lowest fS_2 gave greenish/brown and dark green-bluish coloration.

It is obvious that the silicate colors are functions of oxygen and sulfur fugacities. This is not surprising because both transition elements copper and iron have several valence states and can establish different redox pairs, which give raise to different colors. The intensities of the colors are also in direct relation-

Table 3. Silicate appearance and metal/silicate and metal/sulfide partition coefficients at 1300°C.[a]

Run ID	Silicate appearance	log fO_2	log fS_2	$D^{met/sil}$ Cu	$D^{met/sil}$ Fe	$D^{met/sulf}$ Cu	$D^{met/sulf}$ Fe
No iron, no sulfur (−Fe, −S)							
C-C-1	Clear, transparent	−9.19	N/A[b]	306	N/A	N/A	N/A
C-C-9	Clear, transparent	−10.66	N/A	540	N/A	N/A	N/A
C-C-4	Clear, transparent	−11.34	N/A	917	N/A	N/A	N/A
C-C-3	Very slightly gray, transparent	−12.43	N/A	2439	N/A	N/A	N/A
C-C-2	Slightly gray, transparent	−13.55	N/A	2782	N/A	N/A	N/A
Plus iron, no sulfur (+Fe, −S)							
C-C-1	Intensive dark green, slightly bluish, transparent	−9.19	N/A	276	0.032	N/A	N/A
C-C-9	Intensive medium green, transparent	−10.66	N/A	598	0.702	N/A	N/A
C-C-4	Intensive turquoise, slightly bluish, transparent	−11.34	N/A	991	1.87	N/A	N/A
C-C-3	Less intensive turquoise, slightly bluish, transparent	−12.43	N/A	1265	0.601	N/A	N/A
C-C-2	Less intensive turquoise, slightly bluish, transparent	−13.55	N/A	1819	1.33	N/A	N/A
No iron, plus sulfur (−Fe, +S)							
S-II-5	Colorless, transparent	−9.52	−4.22	295	N/A	1.25	N/A
S-I-2	Pale green	−11.71	−2.84	(793)	N/A	1.25	N/A
S-I-18	Colorless, slightly reddish, transparent	−11.72	−5.27	852	N/A	1.24	N/A
S-I-23	Colorless, slightly reddish, transparent	−11.75	−6.29	—[c]	N/A	—[c]	N/A
S-I-25	Colorless, slightly reddish, transparent	−11.78	−6.29	1124	N/A	1.25	N/A
S-I-22	Colorless, slightly reddish, transparent	−11.83	−6.29	1124	N/A	1.24	N/A
S-I-24	Colorless, slightly reddish, transparent	−11.91	−6.29	—[c]	N/A	—[c]	N/A
S-II-7	Honey yellow, transparent	−12.18	−4.36	1408	N/A	1.26	N/A
S-II-8	Yellow/brownish, transparent	−12.63	−4.36	1852	N/A	1.26	N/A
Plus iron, plus sulfur (+Fe, +S)							
S-I-2	Brown/green inhomogeneous	−11.71	−2.84	(1250)	(0.098)	1.30	0.232
S-I-5	Dark green	−11.86	−2.50	2273	0.086	1.36	0.032
S-II-5	Red-brown, opaque	−9.52	−4.22	480	0.012	1.26	0.111
S-I-14	Red-brown, opaque	−11.74	−4.22	888	0.109	1.41	0.072
S-II-7	Red-brown, opaque	−12.18	−4.36	—[c]	—[c]	—[c]	—[c]
S-II-9	Red-brown, opaque	−12.47	−4.61	1124	0.259	1.39	0.127
S-I-18	Greenish/brown	−11.72	−5.27	1357	0.236	1.31	0.311
S-I-22	Deep dark green/bluish green	−11.83	−6.29	1225	0.359	1.36	0.309

[a] $D^{met/sil}$ and $D^{met/sulf}$ are metal/silicate and metal/sulfide partition coefficients, respectively. All runs are sorted by decreasing oxygen fugacity, except for the runs of system (+Fe, +S), which are sorted by decreasing sulfur fugacity. Partition coefficients in parentheses are not included in the data analyses.

[b] N/A, not applicable.

[c] See Table 2.

ship to the absolute amounts of the elements dissolved in the silicates. The colors should correlate with partition coefficients because both depend on the amount and valence of an element dissolved in the silicate and on the fO_2 and fS_2.

3.3. Thermodynamic Modeling

3.3.1 Determination of the formal valence of an element dissolved in silicate melt

The solubility of a metallic element in silicate liquid as function of oxygen fugacity can be used to calculate its formal valence in the silicate liquid. Silicate melts can be described as ionic solutions of cations and anions. For modeling purposes, we assume that metal cations (M^{x+}) with valence x are dissolved in the silicate and balanced by anionic O^{2-}, which can be expressed as $[M^{x+} + x/2\ O^{2-}]$ or, more conveniently, as oxide "$MO_{x/2}$." The equilibrium distribution of an element between coexisting metal and silicate is exemplified by

$$M_{metal} + \tfrac{x}{4}\ O_2 = [M^{x+} + x/2\ O^{2-}]_{silicate} = MO_{x/2,silicate}, \quad (1)$$

where M is the metallic element and $MO_{x/2}$ represents the dissolved metal oxide in the silicate melt. The equilibrium constant K_1 of reaction 1 is

$$K_1 = a_{MO_{x/2}}/[a_M \cdot (fO_2)^{x/4}], \quad (2)$$

where $a_{M_{Ox/2}}$ and a_M are the activities of the metal oxide in the silicate and the metallic element in the metal phase at a given oxygen fugacity fO_2. Replacing the activities of the metallic element and the metal oxide by $a = X \cdot \gamma$ (X is mole fraction; γ is activity coefficient) and rearranging the equation yields

$$\log (X_M/X_{MO_{x/2}}) = -\tfrac{x}{4} \cdot \log fO_2 - \log K_1 - \log (\gamma_M/\gamma_{MO_{x/2}}). \quad (3a)$$

Partition coefficients are measured as mass concentration ratios and we have to convert mole fractions in Eqn. 3a to mass fractions by use of the expressions

$$X_M = C_M \cdot A \quad (3b)$$

and

$$X_{MO_{x/2}} = C_{MO_{x/2}} \cdot B. \quad (3c)$$

This introduces the formal conversion factors A and B to Eqn. 3a (see Borisov et al., 1994, for more detail). However, these conversions factors can only be taken as constant for systems where no major compositional changes occur in either the silicate or metal (e.g., large changes in FeO contents change the

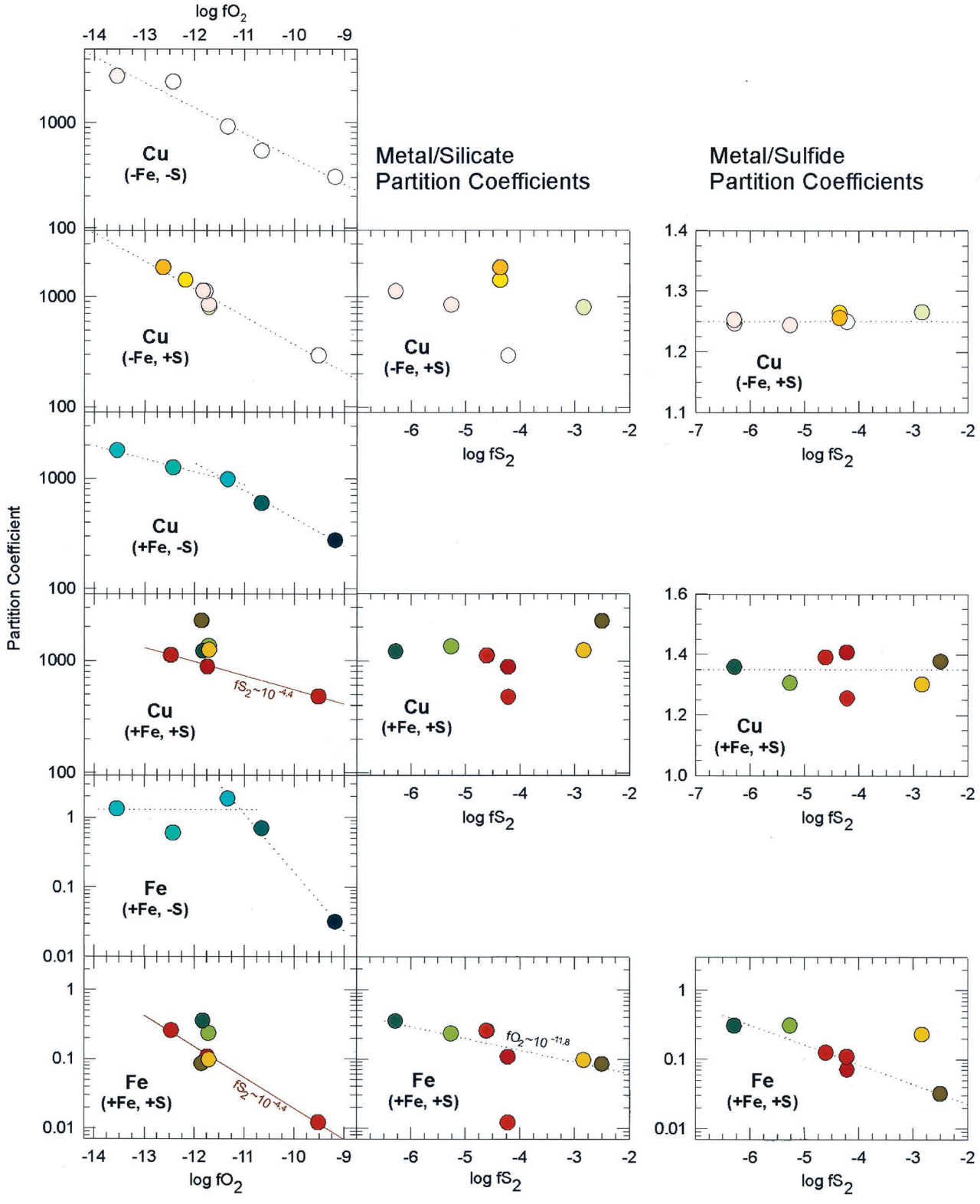

Fig. 2. Metal/silicate partition coefficients (mass concentration ratios) for copper and iron as a function of oxygen fugacity and sulfur fugacity at 1300°C. The first two columns of graphs are for metal/silicate partition coefficients as function of oxygen and sulfur fugacity, respectively. The last column shows metal/sulfide partition coefficients as function of sulfur fugacity. The first four rows show the data for Cu partitioning for the four systems with and/or without iron and sulfur. The last two rows are for the respective iron partition coefficients. Note that metal/sulfide partition coefficients for Cu are not plotted on a log scale. The colors of the symbols are those of the silicates after equilibration. The dotted lines in each plot of Figure 2 represent the best fits for copper and iron $D^{met/sil}$ (or respective $D^{met/sulf}$) as function of fO_2 or fS_2 (Eqn. 9b; see Table 4).

mole fractions of other elements in the silicate). Taking the conversion factors A and B as constant for now, Eqn. 3a becomes

$$\log (C_M/C_{MO_{x/2}}) = -x/4 \cdot \log fO_2 - \log (\gamma_M/\gamma_{MO_{x/2}}) - \log K_1 - \log (A/B), \quad (4a)$$

corresponding to a linear equation

$$\log (C_M/C_{MO_{x/2}}) = c_1 + c_2 \cdot \log fO_2, \quad (4b)$$

where

$$c_1 = -\log [K_1 \cdot (A \cdot \gamma_M)/(B \cdot \gamma_{MO_{x/2}})] \quad (4c)$$

and

$$c_2 = -x/4. \quad (4d)$$

A linear dependence of the element's metal to silicate concentration ratio is expected as a function of log fO_2 as long as Henry's law is obeyed.

Activity coefficients of Cu in liquid CuFe alloys with $X_{Cu} > 0.9$ are close to unity (Maruyama and Ban-ya, 1980; Moser et al., 1985). The activity coefficients of FeO, NiO, and CoO in the silicate melt were found to be independent of oxygen fugacity and temperature (Holzheid et al., 1997). Assuming similar behavior for Cu as oxide in the silicate liquid, we expect a linear relationship when plotting the experimental partition coefficients as a function of oxygen fugacity as indicated by Eqn. 4b. The intercept c_1 contains information about the activity coefficients. The slope c_2 of the best fit line (Eqn. 4b) is a function of the valence state x of the metal oxide ($x = -4 \cdot c_2$, Eqn. 4d) and is used to calculate the formal valence of the element of interest dissolved in the silicate melt.

3.3.2 Metal/Silicate and Metal/Sulfide Partition Coefficients

Metal/silicate partition coefficients $D^{met/sil}$ are defined as mass concentration ratios of an element in the metal phase and in the silicate phase:

$$D^{met/sil} = C_M^{met}/C_{MO_{x/2}}^{sil}. \quad (5)$$

The dependence of $D^{met/sil}$ on oxygen fugacity provides information about the formal valence of a metallic element dissolved as metal oxide $MO_{x/2}$ in the silicate phase, as shown above. Holzheid and Palme (1996) pointed out that it is not sufficient to define a metal/silicate partition coefficient as function of temperature and fO_2 alone. The composition of the metal—because of the likely nonideal behavior of the elemental components in the metal phases—needs to be incorporated. Recalculation of the solubility for an element in the silicate melt coexisting with a metal alloy to the equivalent solubility for a coexisting pure metal must include the effect of metal composition. Consequently, the metal/silicate partition coefficient has a different value depending on the metal composition it is computed from. The experimental metal/silicate partition coefficients here (Table 3) are computed from the metal composition present in the experiments (Table 2). However, the partition coefficients for modeling core formation processes in terrestrial planets must be for partitioning of Cu between an iron alloy (or iron–nickel alloy) and silicate melt. Such an Fe or FeNi alloy only contains trace amounts of Cu, which is different than the metal compositions in the experiments.

Following Holzheid and Palme (1996), the "solubility" metal/silicate partition coefficient is the concentration ratio of an element in the metal to that in the silicate melt. In cases where the metal is "pure," this solubility partition coefficient $D^{met/sil}_{pure\text{-}metal}$ is inverse proportional of the metal solubility in the silicate melt (C^{sil}):

$$D^{met/sil}_{pure\text{-}metal} = 100/C^{sil}. \quad (6a)$$

This partition coefficient $D^{met/sil}_{pure\text{-}metal}$ can be recalculated to a "generic" metal/silicate partition coefficient for an alloy and silicate melt ($D^{met/sil}$) by considering the mole fraction (X), the activity coefficient in the metal alloy (γ^{met}), and the mass-to-mole fraction conversion factor A (see Holzheid and Palme, 1996):

$$D^{met/sil}_{pure\text{-}metal} = 1/C^{sil} = A \cdot \gamma^{met} \cdot C^{met}/C^{sil} = A \cdot \gamma^{met} \cdot D^{met/sil}. \quad (6b)$$

Although activity coefficients of Cu (γ_{Cu}) in Cu-rich CuFe alloys ($X_{Cu} > 0.9$) are close to unity, γ_{Cu} in Fe-rich CuFe alloys reflect a strong nonideal behavior. For example, the activity coefficient of Cu at 1600°C in a liquid CuFe alloy increases from 5.2 ($X_{Cu} = 0.1$) to 8.4 at $X_{Cu} = 0.01$, to 9.0 in an infinitely dilute solution of Cu in Fe (Maruyama and Ban-ya, 1980). At 1300°C in a solid Fe-rich CuFe alloy, $\gamma_{Cu} = 9.2$ for the infinitely dilute solution (Moser et al., 1985). Thus, when comparing experimentally determined partition coefficients from various studies, the nonideal behavior of Cu in the Cu metal alloy needs to be considered. On the other hand, metal/silicate partition coefficients from experiments with different metal compositions can be used to calculate the activity coefficient of the metallic element in the alloy provided that the activity coefficient of the metal oxide dissolved in the silicate melt is constant.

The metal/sulfide partition coefficient $D^{met/sulf}$ is analogously defined as the mass concentration ratio between metal and sulfide:

$$D^{met/sulf} = C_M^{met}/C_{MS_{x/2}}^{sulf}. \quad (7)$$

The variation of $D^{met/sulf}$ as function of sulfur fugacity can be used to calculate the formal valence of an element dissolved in the sulfide phase as $[M^{x+} + x/2\ S^{2-}]_{sulfide}$, or written as sulfide "$MS_{x/2}$." A similar formalism describes element partitioning between sulfide and silicate. In this case, the partition coefficient is expected to depend on both oxygen and sulfur fugacity.

The thermodynamic modeling above explicitly assumes that the dissolved element in the silicate in cationic form is only balanced by O^{2-} (i.e., only oxidic dissolution present), and hence the expected correlation of metal/silicate partition coefficient with oxygen fugacity. Once sulfur is present in addition, we have to expand this type of modeling to consider metals dissolved in oxidic and sulfidic form in the silicate (see Nagamori, 1974). The two contributions to the total of the dissolved element in the silicate are the oxidic form $[M^{x+} + \frac{x}{2} O^{2-}]$ with the cationic valence x and the sulfidic form $[M^{y+} + \frac{y}{2} S^{2-}]$ where the cation has the formal valence y. The equation for metal/silicate equilibrium is

Table 4. Fit coefficients for Cu and Fe metal/silicate (Met/sil) and metal/sulfide (Met/sulf) partition coefficients from this study.[a]

Partition system	c_1	c_2 (for fO_2)	c_3 (for fS_2)	Formal valence	Notes
				In silicate	
Met/sil Cu	+0.23 ± 0.37	−0.24 ± 0.03	N/A	0.96 ± 0.13	−Fe, −S
Met/sil Cu	+0.04 ± 0.29	−0.25 ± 0.03	No depend.	1.00 ± 0.12	−Fe, +S
Met/sil Cu	+0.78 ± 0.25	−0.19 ± 0.02	N/A	0.76 ± 0.08	+Fe, −S, all data
	+0.11 ± 0.23	−0.25 ± 0.03	N/A	1.00 ± 0.12	High fO_2 data; see text
	+1.63 ± 0.16	−0.12 ± 0.01	N/A	0.48 ± 0.04	Low fO_2 data, turquoise silicates; see text
Met/sil Cu	+1.16 ± 0.85	−0.16 ± 0.07	Not fitted	0.64 + 0.28	+Fe, +S, all data excluding run S-I-2
	+1.49 ± 0.04	−0.12 ± 0.01	See notes	0.48 ± 0.04	Constant log $fS_2 \sim -4.4$, red-brown silicates
	+3.41 ± 0.29	See notes	+0.06 ± 0.06	N/A	Constant log fO_2
Met/sil Fe	−9.14 ± 0.72	−0.84 ± 0.07	N/A	3.36 ± 0.28	+Fe, −S, high fO_2 data; see text
	+0.10 ± 0.20	No depend.	N/A	—	Low fO_2 data, turquoise silicates; see text
Met/sil Fe	−6.91 ± 0.51	−0.45 ± 0.04	−0.18 ± 0.04	2.52 ± 0.06	+Fe, +S, excluding run S-I-2
	−6.16 ± 0.19	−0.45 ± 0.02	See notes	1.80 ± 0.08	Constant log $fS_2 \sim -4.4$, red-brown silicates
	−1.55 ± 0.18	See notes	−0.17 ± 0.04	0.68 ± 0.16	Constant log $fO_2 \sim -11.8$
				In sulfide	
Met/sulf Cu	+0.098 ± 0.004	No depend.	No depend.	1.03 ± 0.04	−Fe, +S, valence from stoichiometry; see text
Met/sulf Cu	+0.127 ± 0.020	No depend.	No depend.	1.0	+Fe, +S, valence from stoichiometry; see text
Met/sulf Fe	−2.20 ± 0.22	No depend.	−0.28 ± 0.05	1.12 ± 0.20[b]	+Fe, −S, excluding run S-I-2

[a] All data are for 1300°C. Fit parameters are for $\log D = c_1 + c_2 \cdot \log fO_2 + c_3 \cdot \log fS_2$ (Eqn. 9b). Activity coefficients are averages from individual activity coefficients calculated for each run. N/A, not applicable. No depend., partition coefficients show no apparent dependence on fO_2 or fS_2.
[b] Sulfidic valence is close to two once Cu metal/silicate partitioning is considered; see text.

$$M^0_{metal} + v \cdot {}^x\!/_4\, O_2 + w \cdot {}^y\!/_4\, S_2 = v[M^{x+} + \tfrac{x}{2} O^{2-}]_{silicate} + w[M^{y+} + \tfrac{y}{2} S^{2-}]_{silicate} = v\, MO_{x/2,silicate} + w\, MS_{y/2,silicate}. \quad (8a)$$

Here v and w are the fractional contributions of oxidic and sulfidic form, defined so that v + w = 1. The measured metal/silicate partition coefficient does not distinguish between the concentrations of oxidic and sulfidic form dissolved in the silicate because the overall concentration of the element M is measured in the silicate. We now have to find the thermodynamic relationship between the overall partition coefficient and the oxidic and sulfidic components in the silicate. From the equilibrium constant of reaction 8a, we obtain the relationship of the activities:

$$[a^v_{MO_{x/2}} \cdot a^w_{MS_{y/2}}]_{slicate} = K_{8a} \cdot (fO_2)^{vx/4} \cdot (fS_2)^{wy/4} \cdot [a_M]_{metal}. \quad (8b)$$

Physically, there is no reason to distinguish between balancing M^{x+} by either O^{2-} or S^{2-} species because both anions are freely exchangeable in the silicate melt. Here we assume that both anions have the same valence, so the cation must have the same overall valence (x = y) irrespective of anionic component. Therefore, we set the activities of oxidic and sulfidic components to $a_{MO_{x/2}} = a_{MS_{y/2}}$ in Eqn. 8b. Combining the equilibrium constant, activity coefficients, and conversion factors from mole fractions to mass fractions as done above, we obtain

$$\log D^{met/sil}(M(O,S)_{(x=y)/2}) = \text{constant} - {}^{vx}\!/_4 \log fO_2 - {}^{wy}\!/_4 \log fS_2, \quad (9a)$$

or, more generally,

$$\log D^{met/sil} = c_1 + c_2 \log fO_2 + c_3 \log fS_2. \quad (9b)$$

Here the coefficients are $c_2 = -vx/4$ and $c_3 = -wy/4$. Because we set x = y above, the formal overall valence of M^{x+} is obtained from $x = -4(c_2 + c_3)$. This also allows us to obtain the mass fractions (v, w) of the oxidic and sulfidic components.

It should be noted that any possible dissolution of oxidic or sulfidic species in the metal and/or sulfide phase complicates matters even further. Here we assume that the metal phases do not contain any dissolved oxidic and sulfidic species and that the sulfide phase does not contain any oxidic components. The totals in the sulfide analyses were always close to 100%, and as long as metal is present in the charges, the oxidic species in the sulfide are not expected in significant, if any, amounts.

3.4. Partition Coefficients for Copper and Iron

The calculated metal/silicate partition coefficients and metal/sulfide partition coefficients are given in Table 3. In Figure 2, metal/silicate and metal/sulfide partition coefficients ($D^{met/sil}$, $D^{met/sulf}$) of Cu and Fe are plotted as function of oxygen fugacity and sulfur fugacity at constant temperature of 1300°C. Symbol colors correspond to the observed colors of the silicates. The top four rows of graphs are for copper, and the bottom two rows are for iron. The metal/silicate partition coefficients are plotted as a function of fO_2 (first column of plots) and as function of fS_2 (second column of plots). The third column of plots shows the metal/sulfide partition coefficients as function of sulfur fugacity. The dotted lines in each plot represent the best fits for copper and iron partition coefficients as function of fO_2 or fS_2. The least square fit parameters and calculated formal valences from the fits are listed in Table 4 for all subsets of experiments.

3.4.1 Metal/Silicate Partitioning of Copper and Iron

The metal/silicate partition coefficients of Cu decrease with increasing oxygen fugacity at constant temperature (Fig. 2), consistent with higher Cu solubility in the silicate under more oxidizing conditions. The Cu partition coefficients show no dependence on sulfur fugacities. The calculated valence of Cu

in the silicate melt from the Fe- and S-free experiments at 1300°C is 0.96 ± 0.13, which is close to the valence of unity expected for solution of Cu^+ as $CuO_{0.5}$ (Cu_2O). The correlation of the partition coefficient with oxygen fugacity explicitly implies the presence of monovalent copper balanced by O^{2-} in the silicate melt, i.e., $Cu^+ + 0.5\ O^{2-}$, or "$CuO_{0.5}$." The fit parameters in Table 4 for other subsets of experiments (with Fe and/or S) also indicate formal valences close to unity for Cu, but there are systematic variations in the valences of Cu among these subsets. The best agreement for the observed and expected valence of Cu^{1+} is found in the Fe-free systems, irrespective of the presence of sulfur. The valence for Cu in the silicate is 1.00 ± 0.12 in the Fe-free, S-containing experiments. Within uncertainties, the metal/silicate partition coefficients of Cu are the same and only depend on fO_2. It is known that Cu can dissolve as oxidic and sulfidic species in the silicate (e.g., Nagamori, 1974), but apparently here the fS_2 is too low to allow substantial sulfidic dissolution. Our findings are consistent with the observations described in the glass-making literature that Cu sulfide is practically insoluble at low sulfur fugacities (irrespective of fO_2, e.g., Weyl, 1954). If sulfidic dissolution occurs in addition to oxidic dissolution of Cu in the silicate, metal/silicate partition coefficients in S-bearing experiments should be lower at constant fO_2 and depend on the sulfur fugacity (Eqns. 9a,b), which is not observed (within 1σ uncertainties).

In the Fe-bearing but S-free experiments, the partition coefficients (Fig. 2, third row) show two trends over the entire fO_2 range studied. The data are linear from high fO_2 down to log fO_2 of approximately −11 to −12. At lower fO_2, the data follow a shallower linear relationship with fO_2. The partition coefficients are smaller than expected from the trend seen at higher fO_2. The formal valence of Cu from all data is 0.76 ± 0.08 (see Table 4). A fit of the high fO_2 data only yields a Cu valence of 1.00 ± 0.12, whereas a fit of the low fO_2 data (turquoise silicates) gives a valence of 0.48 ± 0.04. The Cu partition coefficients in the Fe-free systems do not show such curvature at low fO_2, and the valence of Cu is unity over the entire fO_2 range. The change in partitioning behavior must be due to the presence of iron, because this is the only variable changed. We analyze the iron metal/silicate partitioning next.

The iron metal/silicate partition coefficients for the system (+Fe, −S) are plotted in the fifth row in Figure 2. They increase as a function of decreasing oxygen fugacity at higher fO_2 but flatten to approximately constant values at lower fO_2 in the turquoise-colored silicates. The decrease of the metal/silicate partition coefficients for iron correlate with a similar trend observed for copper.

The three data points at higher fO_2 yield a formal valence state of Fe of 3.36 ± 0.28 in the silicate, which is quite unusual. Schmitt et al. (1989) and Holzheid and Palme (1996) investigated the partitioning of iron between iron alloys and silicate as a function of oxygen fugacity. Their results show that divalent iron (presumably as "FeO") is dissolved in silicate melt under oxygen fugacities considered here. However, in contrast to those studies, we have large amounts of copper in the system. The odd behavior of Cu and Fe here indicates that their partitioning is coupled in some manner. Metal cations with two (or more) valence states can affect the Fe^{3+}/Fe^{2+} ratio because charge-transfer reactions can take place (see Schreiber et al., 1992). Redox reactions of Cu^0 and Cu^+ with other polyvalent elements such as Fe, Pb, or Sn have been suggested to explain the coloring of "sunstones" by Hofmeister and Rossman (1985). To explain the presence of Fe^{3+} here, we assume that Fe^{2+} and Cu^+ form by oxidation of the metal, as expected from the previous results. This is followed by the redox reaction

$$Fe^{2+} + Cu^+ = Fe^{3+} + Cu^0. \quad (10)$$

This reaction generates Fe^{3+} from Fe^{2+} at higher oxygen fugacities and may lead to green coloration of the glass by Fe^{3+}.

At oxygen fugacities below log $fO_2 = -12$, Fe^{2+} becomes more stable and the redox reaction 10 is driven to the left side. This could explain the appearance of the turquoise colors because the presence of Fe^{2+} and Fe^{3+} can produce bluer colors (Weyl, 1954). The copper–iron redox reaction 10 also implies that the amount of Cu^+ (or $CuO_{0.5}$) increases (i.e., the metal/silicate partition coefficient decreases) when FeO is more stable. This is consistent with the observations from Table 2 for experiments with and without iron in the sulfur free system. The explanation for the valence below unity for Cu in the turquoise silicates is that the oxidation of Cu metal proceeds via

$$Cu^0 + FeO_{1.5} = FeO + CuO_{0.5} \quad (11)$$

as well as by reaction 1. Reaction 11 is independent of oxygen fugacity. The fitting procedure (Eqn. 4b) considers only that metal is oxidized by O_2 and does not consider additional $CuO_{0.5}$ from redox exchange reactions. Of course, more experiments at low oxygen fugacity are needed to verify this hypothesis, and spectroscopic analyses to determine the valence states of Cu and Fe in these systems are part of future work needed.

The copper metal/silicate partition coefficient in the S- and Fe-bearing experiments (Fig. 2, fourth row) show an increase with decreasing oxygen fugacities. The partition coefficients are somewhat larger when Fe is present than when Fe is absent; see, e.g., runs S-II-5, S-II-2, S-I-18, and S-I-22 in Table 2, which were performed simultaneously. The Cu concentrations in the metal of both sets of experiments are not significantly different, but the amount of copper oxide in the silicate is lower in the Fe-bearing experiments than in the Fe-free ones, so that the metal/silicate partition coefficients are higher in the Fe-bearing system. The smaller Cu abundances are in part caused by "dilution" of the silicate with iron oxide, but this cannot explain the smaller Cu concentrations entirely.

A least square regression analysis of all data plotted in the system (+Fe, +S) yields a formal valence of 0.64 ± 0.28 for Cu in the silicate melt when the data are only plotted as a function of fO_2 (Eqn. 4b, Table 4). However, the plot shows that the experiments done at high and low sulfur fugacities (greenish silicates) have higher metal/silicate partition coefficients than those experiments done at intermediate fS_2 (i.e., the red-brown silicates). A fit of the partition coefficients as a function of oxygen fugacity at constant $fS_2 \sim 10^{-4.4}$ gives a formal valence of 0.48 ± 0.04 (Table 4). This is not significantly different than the value of 0.64 ± 0.28 obtained from a fit from all data here but is clearly below the expected valence of unity. A plot of the metal/silicate partition coefficients as a function of sulfur fugacity in the system +Fe, +S (fourth row, second column of Fig. 2) reveals no apparent dependence on

fS_2. This is also seen from the fit parameters of the metal/silicate partition coefficients as a function of fS_2 at constant fO_2 in Table 4. Again, the absence of dissolved sulfidic Cu is consistent with the very low solubility of Cu_2S in silicate melts (e.g., Weyl, 1954).

The formal valence of ~0.5 for copper in the silicate system (+Fe, +S) is similar to that in the system (+Fe, −S) at low oxygen fugacities. This valence of Cu probably results from the presence of iron because it is close to unity in the Fe-free experiments. Therefore, we analyze the iron distribution between metal and silicate.

The silicates from the S-free experiments typically contain half as much iron as the silicates from the S-bearing experiments. For example, at about the same oxygen fugacity, we find 2.1% Fe in the silicate in a S-free experiment (run C-C-4, log $fO_2 = -11.34$) but 4.0% Fe in a S-bearing experiment (run S-I-14, log $fO_2 = -11.74$, log $fS_2 = -4.22$). This suggests that the presence of sulfur leads to increasing solubility of Fe in silicate melts. However, the measured S concentrations in the silicate glass of the Fe-bearing experiments of <0.04% are below the amount expected for substantial Fe-S solution in the silicate melt. For example, if the additional 2% of Fe in the silicate were due to sulfidic dissolution, we would expect sulfur concentrations of ~1% in the silicate, compared with the <0.04% seen. We cannot rule out the possibility that sulfur was lost from the silicate melt during cooling, but the loss needed is fairly large, whereas cooling times were short. Still, the higher Fe concentrations in silicates of S-bearing experiments must be related to the presence of sulfur, because other parameters, such as the oxygen fugacity, can be ruled out.

In the Cu, Fe, and S-bearing system, the metal/silicate partition coefficient of Fe increases with decreasing oxygen fugacity *and* decreasing sulfur fugacity (Fig. 2, bottom). The Fe metal/silicate partition coefficients at approximately constant fO_2 are somewhat higher when sulfur is absent and partition coefficients increase with decreasing sulfur fugacity (Table 2). The fit parameters for iron metal/silicate partition coefficients as function of fO_2 at constant fS_2 (and vice versa) are given in Table 4. We also fitted the partition coefficients as a function of fO_2 and fS_2 according to Eqn. 9 to test the presence of sulfidic and oxidic Fe in the silicate. This yields an overall valence for Fe of 2.52 ± 0.06 and indicates the presence of Fe^{2+} and Fe^{3+} in the melt, as found above for the Fe-bearing and S-free system.

It is known that sulfur can interact with the silicate melt and cause oxidation of Fe^{2+} to Fe^{3+}. The dissolution of sulfide and its effect on the Fe^{2+} to Fe^{3+} ratio is used for glass amber coloring. This is nicely illustrated by Schreiber et al. (1992), who show the intensity of glass colors as a function of oxygen and sulfur fugacity. This effect is utilized in industrial glass coloring. Iron sulfide–containing glasses are used for the black colored marble effects in Bohemian glasses (Weyl, 1954). We observe more intense coloring in the S- and Fe-bearing experiments than in those without iron. The silicates from the Fe- and S-bearing experiments done under intermediate fS_2 are dark reddish-brown opaque glasses, whereas in experiments with sulfur fugacities below log $fS_2 < -5$ and above log $fS_2 > -3$ gave dark greenish glasses. The opaque reddish-brown glasses were not seen in the S-free experiments. Winther et al. (1998) report that poly-sulfur anions $(S_2)^-$ and $(S_3)^-$ dissolved in albite melt cause violet coloring, and something similar could occur here. To explain the higher iron content in the system (+Fe, +S), we write an Fe^{2+}-Fe^{3+} redox reaction involving sulfur

$$[2\ Fe^{2+}]_{silicate} + 0.5\ S_2 = [2Fe^{3+}]_{silicate} + [S^{2-}]_{silicate}. \quad (12a)$$

The net effect of such a reaction is that the Fe^{3+}/Fe^{2+} ratio increases and more sulfidic iron is dissolved in the silicate with increasing sulfur fugacity. At the same time, the reaction

$$Fe^0_{metal} + 0.5\ O_2 = [Fe^{2+}]_{silicate} + [O^{2-}]_{silicate} \quad (12b)$$

occurs. The overall partitioning of iron between metal and silicate from Eqns. 12a,b and the fit coefficients in Table 4 is

$$Fe^0_{metal} + 0.45\ O_2 + 0.18\ S_2 = [Fe^{2.52+} + 0.90\ O^{2-} + 0.36\ S^{2-}]_{silicate}. \quad (13)$$

The overall valence of $Fe^{2.52+}$ indicates that approximately half of the iron is Fe^{2+} and half is Fe^{3+}(48% Fe^{2+} and 52% Fe^{3+}). Our assumption is that the anions $O^{2-}$and S^{2-} both balance Fe^{2+} and Fe^{3+}. The fractions of oxidic (0.71) and sulfidic (0.29) iron are obtained from the fit coefficients and Eqns. 9a,b. However, the amount of sulfidic iron suggests that that there should be around 0.5 to 1% sulfur in the silicate, which was not observed. This can be explained by the abundant copper in the system so that another equilibrium affects iron metal/silicate partitioning. Any iron sulfide in the silicate may convert to copper sulfide, which does not dissolve in the silicate, and the iron remains in the silicate as oxide

$$CuO_{0.5} + 0.5\ FeS = CuS_{0.5} + 0.5\ FeO. \quad (14)$$

This reaction is independent of fO_2 and fS_2 and does not enter into analyses the dependence of partition coefficients on oxygen and sulfur fugacities. We substitute Eqn. 13 into Eqn. 14 to obtain

$$Fe^0_{metal} + 0.72\ [CuO_{0.5}]_{silicate} + 0.45\ O_2 + 0.18\ S_2 = [Fe^{2.52+} + 1.26\ O^{2-}]_{silicate} + 0.72\ [CuS_{0.5}]_{sulfide}. \quad (15)$$

Reaction 15 has the effect of oxidizing iron metal to Fe^{2+} and Fe^{3+} in the silicate ("$Fe_3O_{3.78}$") and decreasing the amount of copper oxide in the silicate by sulfide formation, both consistent with the observations. The low formal valence obtained from the fit of the Cu metal/silicate partition coefficient vs. fO_2 is then explained by the occurrence of reaction 14, which shows that the Cu abundance in the silicate is not only governed by the oxidation of metal alone (Eqn. 1). The coupling of the copper and iron partitioning reactions explains the dependence of the iron metal/silicate partition coefficient on the sulfur fugacity despite the absence of significant amounts of sulfur observed in the silicate.

3.4.2 Metal/Sulfide Partitioning of Copper and Iron

The metal/sulfide partition coefficients for Cu and Fe are plotted as a function of sulfur fugacity in Figure 2 (last column). In contrast to all other partition coefficients shown in Figure 2, the Cu metal/sulfide partition coefficients are plotted on a *linear* scale. The Cu metal/sulfide partition coefficients are independent of sulfur fugacity and are constant at 1.25 ± 0.01

(−Fe, +S) or 1.34 ± 0.06 (+Fe, +S). The metal/sulfide partition coefficients are somewhat larger in the Fe-bearing system because the absolute concentration of Cu in the copper–iron sulfide is smaller than in the metal phase. The Cu partition coefficients are independent on sulfur fugacity because Cu is distributed between two pure phases (Cu metal and Cu sulfide). The partition coefficient must be constant as long as sulfur fugacities are high enough to stabilize the sulfide phase. Copper–sulfur phase diagram studies show that the equilibrium partial pressure of sulfur over copper-saturated Cu_2S at 1300°C is log $fS_2 = -5.37$ (e.g., Bale and Toguri, 1976). Most of our experiments in the S-bearing systems were conducted at higher sulfur fugacities, which means that Cu sulfide formed. The EMP and XRD analyses confirmed the presence of Cu_2S, indicating a formal valence of Cu^{1+} in these sulfide melts. This was found for Cu sulfide in the Fe-free and Fe-bearing systems. Given longer experimental duration, eventually all Cu metal is transformed to Cu_2S if the fS_2 is higher than that of the Cu/Cu_2S phase boundary. Here the experiments were stopped before the sulfide formation reached completion. However, the remaining metal is in equilibrium with the sulfide and silicate because diffusion in these phases is faster than rate of sulfide formation.

The iron metal/sulfide partition coefficients in the system (+Fe, +S) show a clear dependence on sulfur fugacity (Fig. 2, bottom right) and the data (excluding runs S-I-2) yield the regression

$$\log D^{met/sulf}(Fe) = -2.20(\pm 0.22) - 0.28(\pm 0.05) \log fS_2. \quad (16)$$

This translates to a formal valence of 1.12 ± 0.20 for Fe and indicates the presence of "$FeS_{0.56}$" in the Cu-Fe sulfide. The EMP analyses indicate an average stoichiometry of about $(Cu_{0.94 \pm 0.05}Fe_{0.06 \pm 0.03})S_{0.55 \pm 0.02}$ or $0.94\,CuS_{0.5} + 0.06\,FeS$ for all sulfides in this set of experiments, compared to $CuS_{0.5}$ in the Fe-free ones. The sulfide stoichiometry is consistent with the presence of divalent Fe as FeS, whereas the formal valence from the fit is 1.12. However, the apparent presence of $FeS_{0.56}$ in the sulfide and the overall sulfide composition of $(Cu_{0.94}Fe_{0.06})S_{0.55}$ could indicate that the Fe and Cu exchange reactions between metal and sulfide are coupled. The exchange reaction can be expressed as

$$[Cu^+(S^{2-})_{0.5}]_{sulfide} + Fe^0_{metal} + 0.25\,S_2 = Cu^0_{metal} + [Fe^{2+}S^{2-}]_{sulfide}. \quad (17)$$

Following the formalism above (Eqns. 2–4), the metal/sulfide partition coefficients are related via

$$\log D^{met/sulf}(Fe) = \text{constant} + \log D^{met.sulf}(Cu) - 0.25 \log fS_2. \quad (18a)$$

The metal/sulfide partition coefficient of Cu is constant and thus

$$\log D^{met/sulf}(Fe) = \text{constant} - 0.25 \log fS_2. \quad (18b)$$

The constant in Eqns. 16 and 18b also contains the value of the Cu metal/sulfide partition coefficient, which has to be considered when deriving activity coefficients. The observed fit coefficient −0.28 ± 0.05 for log fS_2 in Eqn. 16 is consistent with that expected from Eqn. 18b and supports the argument that the Fe and Cu metal/sulfide exchange reactions are coupled. In addition, it can be shown that the activities of FeS in $CuS_{0.5}$ are above unity if the $Cu/CuS_{0.5}$ equilibrium is not considered in the evaluation of the activity coefficient from reaction 16. However, activities above unity at 1 bar pressure are thermodynamically impossible.

3.4.3 Dependence of Cu Metal/Silicate Partition Coefficients on Temperature

The variation of Cu metal/silicate partition coefficients with temperature in the S-free systems is illustrated in Figure 3a. Copper metal/silicate partition coefficients decrease (i.e., Cu solubility in the silicate melt increases) with increasing temperature within the experimental temperature range of 1300°C to 1515°C regardless of whether the charges were Fe-free or Fe-bearing. Theoretical modeling predicts that log $D^{met/sil}$ varies proportional to 1/T provided that (a) oxygen fugacities are kept at a constant value (expected increase in $D^{met/sil}$) or are kept in constant relation to a buffer (expected decrease in $D^{met/sil}$) and (b) activity coefficients are temperature independent. Our data are for oxygen fugacities of about half a log unit below the IW buffer. As seen from Figure 3a, the log $D^{met/sil}$ is not linear with 1/T and we expand the fit to

$$\log D^{met/sil}(Cu) = c_4 + c_5 \cdot 10^4/T + c_6 \cdot T, \quad (19)$$

where T is the temperature in kelvin. Least square fit parameters for regressions of all data and the two subsets (Fe-free, Fe-bearing) are listed in Table 5. The additional term $c_6 \cdot T$ is needed to describe the temperature dependence of metal/silicate partition coefficient. As discussed below, the activity coefficients of $CuO_{0.5}$ increase with the silicate's CaO and Al_2O_3 content. We find strong increases in the Al_2O_3 content in the silicates with increasing temperature (from ~16 wt% at 1300°C to 35 wt% at 1515°C; see Fig. 3b) caused by Al_2O_3 uptake from the alumina crucibles used. Because of this change in overall composition, the CaO content decreases from ~23 wt% (1300°C) to 18 wt% (1514°C). These compositional changes are linear with temperature, and therefore the term $c_6 \cdot T$ reflects the temperature dependent change in alumina and lime contents of the silicate melt, which in turn affects the activity of $CuO_{0.5}$, as seen in Figure 5 and discussed below.

Toguri and Santander (1972), Altman and Kellogg (1972), and Reddy and Acholonu (1984) reported decreasing Cu solubility in silicate melt with increasing temperature, as expected for oxygen fugacities kept at a constant value and constant silicate compositions. In our study, we expected an increase in Cu solubility (decrease in metal/silicate partitioning) because the fO_2 was held constant relative to the IW buffer.

3.5. Activity Coefficients

3.5.1. Activity Coefficients for Copper Oxide in the Silicate

The activity coefficient $\gamma_{MO_{x/2}}$ of a metal oxide in the silicate is obtained from Eqns. 4a and 4b and the experimental data by using

$$\log \gamma_{MO_{x/2}} = c_1 + \log(A/B) + \log K + \log \gamma_M. \quad (20)$$

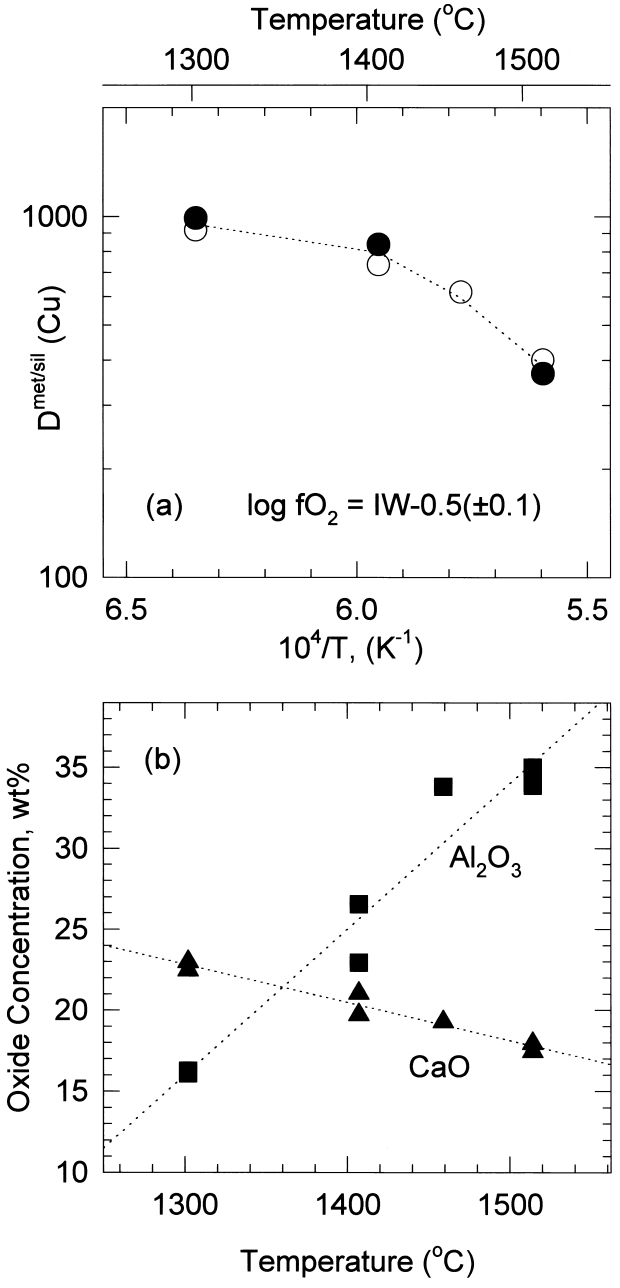

Fig. 3. (a) Temperature dependence of metal–silicate partition coefficients of Cu in silicate melt at an oxygen fugacity corresponding 0.5(±0.1) log units below the IW buffer. Only data for S-free systems are shown. Open circles are for Fe-free systems and closed circles are for Fe-bearing systems. In both systems, log $D^{met/sil}$ decreases with temperature. The decrease of log $D^{met/sil}$ is not linear with 1/T, indicating the apparent dependence of activity coefficients of $CuO_{0.5}$ on temperature. (b) CaO and Al_2O_3 concentrations in the silicates after equilibration. The silicates pick up alumina from the corundum crucibles. This is the cause for the nonlinear temperature dependence with 1/T in Figure 3a above (see text).

This equation can only be used for systems where no redox or oxide/sulfide exchange reactions are involved and only the metal to metal oxide equilibria are relevant. Once other reactions become important, the equilibrium constants for these reactions must be included. This complicates matters significantly because the equilibrium constants and exact stoichiometry of the reactions must be known. Here we restrict the evaluation of the activity coefficients to systems where the formal valence is consistent with the metal oxide equilibria from Eqn. 1. This includes all sets of experiments for which we found copper valences of unity (see Table 4). No attempts are made to evaluate the activity coefficients of iron because of the complexity of the systems discussed above.

Table 5. Temperature dependence of Cu metal/silicate partition coefficients.[a]

System	c_4	c_5	c_6
All data	64.31 ± 11.71	−4.89 ± 0.98	−0.019 ± 0.003
Fe-free	53.07 ± 14.50	−3.98 ± 1.21	−0.016 ± 0.004
Fe-bearing	76.74	−5.91	−0.023

[a] S-free systems only; log oxygen fugacity range relative to iron–wüstite (IW) is IW-0.5 to IW-06. Coefficients are for log $D^{met/sil}(Cu) = c_4 + c_5 \cdot 10^4/T + c_6 \cdot T$; temperature T in kelvin.

The constants c_1 needed for Eqn. 20 are listed in Table 4. To derive activity coefficients, the mass concentration partition coefficients must be transformed to mole fraction ratios (Eqns. 3b, 3c, and 6b). Irrespective of system chosen (S-free, Fe-free or not), the metal/silicate mole fraction ratios are related to the metal/silicate partition coefficients by

$$(X_{Cu,metal}/X_{CuO_{0.5},\,silicate}) = 1.062(\pm 0.020) \cdot D^{met/sil}(Cu) \quad (21a)$$

$$(X_{Fe,metal}/X_{Fe(O,S),\,silicate}) = 1.045(\pm 0.020) \cdot D^{met/sil}(Fe). \quad (21b)$$

This validates the assumption of constant conversion factors for mass to mole fractions in Eqns. 3b,c above. Then the conversion factors in Eqn. 20 are log (A/B) = 0.026(±0.008) for Cu and 0.019(±0.008) for Fe. At 1300°C, the equilibrium constant is log $K(CuO_{0.5})$ = 0.847 (Chase, 1998).

The activity coefficient of Cu metal is taken as unity because essentially pure Cu metal coexists with the silicate melt. The activity coefficient of copper in the silicate melt referenced to pure $CuO_{0.5}$ liquid is then

$$\log \gamma_{CuO_{0.5}} = c_1 + 0.873(\pm 0.008). \quad (22)$$

The activity coefficients derived for $CuO_{0.5}$ in the Fe-free systems are 12.7 (−S) and 8.2 (+S), and these activity coefficients are uncertain within a factor of two. In the Fe-bearing but S-free system, we derive $\gamma_{CuO_{0.5}}$ = 9.6 (uncertainty factor 1.7) from the data at higher fO_2 (see Table 4). We also computed the activity coefficients individually from each run in the different systems. The averages for the activity coefficients obtained this way are 10.7 ± 2.0 (−Fe, −S), 9.0 ± 0.8 (−Fe, +S), and 10.7 ± 0.7 (+Fe, −S; high fO_2 data). The activity coefficients from the fitting procedures result in comparable values, but with larger uncertainties. In conclusion, we recommend an activity coefficient of $\gamma_{CuO_{0.5}}$ = 10 ± 1 from the average of the three values at 1300°C for the silicate compositions employed here.

3.5.2. Activity Coefficient of Iron Sulfide in Copper Sulfide

We use our metal/sulfide partition coefficients to derive the activity coefficient of FeS in $CuS_{0.5}$. The activity coefficient γ_{FeS} is related to the fit coefficient c_1 by

$$c_1 = -\log K_R - \log (A/B)_{Fe} + \log D^{met/sulf}(Cu) + \log (A/B)_{Cu} + \log (\gamma_{Cu^0}/\gamma_{CuS_{0.5}}) + \log \gamma_{FeS} - \log \gamma_{Fe^0}. \quad (23)$$

The equilibrium constant K_R for reaction 17 is $\log K_R = 0.784$ at 1300°C (Bale and Toguri, 1976; Chase, 1998) and γ^0_{Fe}, γ^0_{Cu}, $\gamma_{CuS_{0.5}}$ are the activity coefficients of Fe and Cu in the metal, and $CuS_{0.5}$ in the sulfide. The conversion factors from mass to mole fractions for Fe and Cu, $(A/B)_{Fe}$, and $(A/B)_{Cu}$, are retrieved from the relations of mole fraction ratios and metal/sulfide partition coefficients $(X^0_{Fe}/X_{FeS}) = 0.786(\pm 0.010) \cdot D^{met/sulf}(Fe)$ and $(X^0_{Cu}/X_{CuS_{0.5}}) = 0.792(\pm 0.011) \cdot D^{met/sulf}(Cu)$. The sulfide mole fractions are defined so that $X_{CuS_{0.5}} + X_{FeS} = 1$. The activity coefficient for Cu and $CuS_{0.5}$ are taken as unity. Inserting into Eqn. 23 yields

$$\log \gamma_{FeS} = c_1 + 0.654(\pm 0.032) + \log \gamma_{Fe^0}. \quad (24)$$

The activity coefficient of Fe in CuFe alloys with $X_{Cu} > 0.97$ is 22.7 at 1300°C (Moser et al., 1985). The final result here, using $c_1 = -2.20(\pm 0.22)$ from Table 4, is $\gamma_{FeS} = 0.65$. This value has an uncertainty factor of 1.7, mainly from the uncertainty in the fit parameter c_1. A calculation of the activity coefficients from the individual experiments yields an average $\gamma_{FeS} = 0.998 \pm 0.340$. Bale and Toguri (1976) find that the Temkin (i.e., simple ideal mixing) model and random mixing adequately describe the activities of Cu_2S and FeS in the Cu-Fe-S system. Thus we can compute activity coefficients independently for the sulfide compositions. The Temkin model and random mixing model for the activities are in reference to sulfide compositions where mole fractions are defined for Cu_2S and FeS, whereas here we use mole fractions defined for $CuS_{0.5}$ and FeS. The activities in the Cu_2S and FeS system are different than those referenced to the $CuS_{0.5}$ and FeS system (see Nagamori, 1974) because the mole fractions are defined differently. Taking these differences into account and referring the activity coefficients to the $CuS_{0.5}$ and FeS system, we obtain the activity coefficients from the individual run compositions via the Temkin model as $\gamma_{FeS} = 0.99 \pm 0.03$, and random mixing yields $\gamma_{FeS} = 0.91 \pm 0.04$. We conclude that the activity coefficient of FeS in the system $CuS_{0.5}$ and FeS can be taken as $\gamma_{FeS} = 1$ for $X_{FeS} < 0.1$ at 1300°C.

4. COMPARISON OF THE RESULTS WITH LITERATURE DATA

Literature data and notes about Cu and Fe metal/silicate partition coefficients in sulfur-free systems are summarized in Table 6.

4.1. Copper Valences

Most studies derive monovalent Cu in silicate melts for oxygen fugacities that are within the range of fO_2 used here. Our data are consistent with the formal valences of unity, except for the formal valences of ~0.5 at very low oxygen fugacities in the system (+Fe, −S). In all other studies rich in copper and iron, the lowest oxygen fugacity at 1300°C is $fO_2 \sim 10^{-11}$, which is about the lowest fO_2 for which a valence of unity for Cu is obtained here (see Fig. 2, third row). The formal valence becomes smaller at lower oxygen fugacities.

A formal valence of 1.24 for Cu in silicate melt is obtained from the data of Altman (1978), who studied partitioning between Cu-Au alloys and iron silicates containing CaO and Al_2O_3. The oxygen fugacities of his experiments are much higher than those in the other studies, and a contribution of Cu^{2+} is likely. Ripley and Brophy (1995) obtain a valence of 1.24 from a fit of their six data points. Because the data correlate well, data scatter cannot explain this higher valence. The higher valence also cannot be explained by the oxygen fugacity, which is as low as in other studies yielding valences of unity.

The Cu partitioning results of Schmitt et al. (1989) give a formal valence of 1.52 ± 0.04, which could suggest a contribution by divalent Cu in the silicate melt. This is surprising, because at the low oxygen fugacities employed in their study, monovalent Cu is expected, as found here and in other studies. The presence of sodium and potassium in the silicates used in studies by Ripley and Brophy (1995) and Schmitt et al. (1989) may give a possible solution to these puzzling higher valences. The formal Cu valence is plotted as a function of molar Na + K content in the silicates in Figure 4, which shows that the valence varies linearly with the alkali content. Alkali element ions (e.g., Na^+) can combine with Fe^{3+} ions to form $(FeNa)^{4+}$ polycations in silicate melts with high basicity (e.g., Turkdogan, 1983). This causes the Fe^{3+}/Fe^{2+} ratio to increase in the silicate melt. Higher Fe^{3+} concentrations then move the redox equilibrium $Cu^+ + Fe^{3+} = Fe^{2+} + Cu^{2+}$ toward larger amounts of Cu^{2+} in the melt. Such a reaction may account for the correlation of higher formal Cu valences with higher alkali element content. This mechanism involves alkali elements *and* iron–copper redox equilibria. The experiments of Johnston and Chelko (1966) show that the presence of iron is required because they find a valence of unity for Cu in their sodium silicate that is devoid of other major element oxides. It would be interesting to know more about the iron partitioning in the experiments of Ripley and Brophy (1995), but no analytical details about silicate and metal phase compositions are given in their article. The data of Schmitt et al. (1989) give Fe valences around two. In their system, the total Cu abundances were in the part per million or part per billion range, and only very small amounts of Fe^{3+} were needed to drive the redox reaction for Cu. Clearly more experimental studies are required to investigate the formal valence of Cu as a function of iron and alkali content and basicity of the melt.

4.2. Copper Oxide Activity Coefficients

There are notable variations in the fit coefficient c_1 from the different studies in Table 6, which reflect the activity coefficients of Cu in the metal and of copper oxide in the silicate (Eqns. 3 and 4). This coefficient should be similar for all studies done at the same temperature, if activity coefficients are independent of alloy and silicate composition, and if conversion factors from mass to mole fractions are comparable (see Eqn. 4). The latter factor is typically small; the major variations are from the activity coefficients. In silicate systems equilibrated with pure Cu metal, only the activity coefficient of $CuO_{0.5}$ in the silicate can cause variations, and theoretically a larger coefficient c_1 implies $CuO_{0.5}$ activity coefficients above unity. If the activity coefficient of Cu in a metal alloy is below

Table 6. Fit coefficients for Cu and Fe metal/silicate (Met/sil) partition coefficients from the literature and from the present study.[a]

Partition coefficient system	c_1	c_2 (for fO_2)	Formal oxidic valence	Notes
Met/sil Cu	-0.17 ± 0.50	-0.22 ± 0.04	0.88 ± 0.16	Johnston and Chelko (1966), 1100°C, Cu metal, $Na_2O \cdot 2SiO_2$ melt, no Fe, Al, Ca, Mg oxides, log $fO_2 = -10.25$ to -14.25.
Met/sil Cu	$+0.25 \pm 0.08$	-0.20 ± 0.01	0.80 ± 0.04	Ruddle et al. (1966), 1300°C, Cu-(Fe) metal, SiO_2-saturated Fe-silicate, Fe^{2+}/Fe^{3+} in slag, no Al, Ca, Mg oxides, log $fO_2 = -6$ to -11.
Met/sil Cu	-0.40 ± 0.06	-0.27 ± 0.01	1.08 ± 0.04	Altman and Kellogg (1972), 1286°C, Cu-Au-Fe metal, SiO_2-sat. melt, Fe^{2+}/Fe^{3+} in slag, no Al, Ca, Mg oxides, log $fO_2 = -5.8$ to -8.7.
Met/sil Cu	-0.63 ± 0.07	-0.25 ± 0.01	1.00 ± 0.04	Altman (1978), ~1250°C, Cu-Au-Fe metal, SiO_2-sat. melt, Fe^{2+}/Fe^{3+} in slag, Al_2O_3 ~7 to 8 wt%, no Ca, Mg oxides, log $fO_2 = -6$ to -11.
Met/sil Cu	-0.342 ± 0.006	-0.267 ± 0.001	1.07 ± 0.004	Reddy and Acholonu (1984), 1300°C, Cu metal, alumina sat. Fe silicate, Fe^{2+}/Fe^{3+} in slag, Al_2O_3 11–16 wt%, no Ca, Mg oxides, log $fO_2 = -8$ to -10.
Met/sil Cu	-0.24 ± 0.16	-0.23 ± 0.02	0.92 ± 0.08	See and Rankin (1983), 1300°C, Cu metal, SiO_2-undersaturated Fe silicate, $Al_2O_3 \sim 16$ wt%, no Ca, Mg oxides, log $fO_2 = -7$ to -9.
Met/sil Cu	-0.83 ± 0.07	-0.29 ± 0.01	1.16 ± 0.04	Altman (1978), ~1250°C, Cu-Au-Fe metal, SiO_2-sat. melt, Fe^{2+}/Fe^{3+} in slag, CaO ~ 8 wt%, no Al, Mg oxides, log $fO_2 = -6$ to -10.
Met/sil Cu	-1.02 ± 0.11	-0.31 ± 0.02	1.24 ± 0.08	Altman (1978), ~ 1250°C, Cu-Au-Fe metal, SiO_2-sat. melt, Fe^{2+}/Fe^{3+} in slag, CaO ~ 4.5 wt%, Al_2O_3 ~ 2.7 wt%, no Mg oxides, log $fO_2 = -6$ to -7.3.
Met/sil Cu	$+0.23 \pm 0.37$	-0.24 ± 0.03	0.96 ± 0.13	Present study, 1300°C, Cu metal, Fe-free silicate, Al_2O_3 16 wt%, CaO 23 wt%, MgO 10 wt%, log $fO_2 = -9.2$ to -13.55 (see Table 6).
Met/sil Cu	-0.11 ± 0.23	-0.25 ± 0.03	1.00 ± 0.12	Present study, 1300°C, Cu-metal, Fe-bearing silicate, Al_2O_3 16 wt%, CaO 22 wt%, MgO 10 wt%, log $fO_2 = -9.2$ to -11.3 (see Table 6).
Met/sil Cu	-0.31 ± 0.04	-0.31 ± 0.004	1.24 ± 0.02	Ripley and Brophy (1995), 1245°C, Cu-metal, starting silicates: CaO ~ 11.5, Al_2O_3 ~ 15.5 and 17.9 wt%, Na_2O ~ 1.7 K_2O ~ 0.15 wt%; Fe in silicate, log $fO_2 = -7.9$ to -11.9.
Met/sil Cu	-2.98 ± 0.18	-0.38 ± 0.01	1.52 ± 0.04	Schmitt et al. (1989), 1300°C, Fe-(Ni) metal, starting silicate CaO 9.4 wt%, Al_2O_3 13.1 wt%, Na_2O 2.7 wt%, K_2O 1.8 wt%, Fe in silicate, log $fO_2 = -11.3$ to -13.3.
Met/sil Fe	-5.35 ± 0.34	-0.31 ± 0.04	1.24 ± 0.16	Ruddle et al. (1966), 1300°C, Cu-(Fe) metal, SiO_2-sat. Fe oxide melt, Fe^{2+}/Fe^{3+} in slag, no Al, Ca, Mg oxides, log $fO_2 = -6$ to -11.
Met/sil Fe	-6.83 ± 0.15	-0.49 ± 0.02	1.96 ± 0.08	Altman and Kellogg (1972), 1286°C, Cu-Au-Fe metal, SiO_2-sat. melt, Fe^{2+}/Fe^{3+} in slag, no Al, Ca, Mg oxides, log $fO_2 = -5.8$ to -8.7.
Met/sil Fe	-7.06 ± 0.23	-0.49 ± 0.03	1.96 ± 0.12	Altman (1978), ~1250°C, Cu-Au-Fe metal, SiO_2-sat. melt, Fe^{2+}/Fe^{3+} in slag, Al_2O_3 ~7 to 8 wt%, no Ca, Mg oxides, log $fO_2 = -8$ to -11.
Met/sil Fe	-9.04 ± 0.27	−0.72–0.03	2.88 ± 0.12	Altman (1978), ~1250°C, Cu-Au-Fe metal, SiO_2-sat. melt, Fe^{2+}/Fe^{3+} in slag, CaO ~ 8 wt%, no Al, Mg oxides, log $fO_2 = -8$ to -10.
Met/sil Fe	-9.14 ± 0.72	-0.84 ± 0.07	3.36 ± 0.28	Present study, 1300°C, Cu metal, Fe-bearing silicate, Al_2O_3 16 wt%, CaO 22 wt%, MgO 10 wt%, log $fO_2 = -9.2$ to -11.3 (see Table 6).
Met/sil Fe	-4.40 ± 0.06	-0.48 ± 0.01	1.92 ± 0.04	Holzheid and Palme (1996), 1403°C FeCo and FeNi Alloys, silicates as in present study (see Table 1), log $fO_2 = -8.1$ to -12.6.
Met/sil Fe	-4.43 ± 0.15	-0.44 ± 0.01	1.76 ± 0.04	Schmitt et al. (1989), 1300°C, Fe-(Ni) metal, starting silicate CaO 9.4 wt%, Al_2O_3 13.1 wt%, Na_2O 2.7 wt%, K_2O 1.8 wt%; Fe in silicate, log $fO_2 = -11.3$ to -13.3.

[a] All systems are sulfur-free and listed in order of increasing silicate complexity. Fit parameters are for $\log D = c_1 + c_2 \cdot \log fO_2$. sat., saturated. When data were not presented in parameter form, we fitted the data according to Eqn. (4b), as done for our data in Table 4.

unity, the coefficient c_1 increases, whereas metal activity coefficients above unity decrease c_1.

The activity coefficients given in the literature and our results are compared in Figure 5. The activity coefficients of $CuO_{0.5}$ increase with increasing amounts of CaO and Al_2O_3 in the silicate, and this trend is reflected in the coefficient c_1 in Table 6.

The work by Ruddle et al. (1966) and Taylor and Jeffes (1975) allow us to derive activity coefficients for $CuO_{0.5}$ in silica-saturated iron silicates free of other oxide additions. Activity coefficients in iron (fayalitic) silicates with and without additions of MgO, CaO, and Al_2O_3 at 1300°C have been investigated by Elliot et al. (1978), See and Rankin (1983), and Reddy and Acholonu (1984). The literature activity coefficients are generally lower than the values obtained here, but our silicate systems have higher CaO *and* Al_2O_3 concentrations than the silicates from the literature. The literature studies conclude that lime additions have the strongest effect in suppressing the solubility of $CuO_{0.5}$ in silicate melts, meaning that activity coefficients become larger (and metal/silicate partition coefficients increase). This is shown in Figure 5a, where we plotted the activity coefficients as a function of CaO content. Alumina additions have a similar, although less pronounced, effect. We find that the variation of the $CuO_{0.5}$ activity coefficients in the silicates can be described as a function of mass percentage (CaO $+0.5$ Al_2O_3) in the silicate melts at ~1300°C (Fig. 5b). Despite the differences between the studies (overall oxygen fugacities, silicate type, metal compositions), the $\gamma_{CuO_{0.5}}$ values show a linear increase with (CaO + 0.5 Al_2O_3) that is indicated by the dotted regression line in Figure 5b. Our silicates are less Fe rich but contain much more MgO than the silicates used in the metallurgical stud-

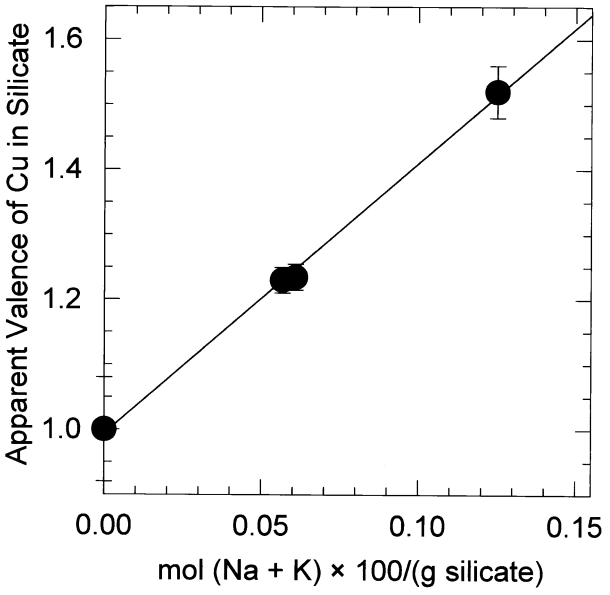

Fig. 4. Apparent variation of the Cu valence in the silicate as a function of molar Na and K content of the silicate. The system here is free of alkali elements and the formal valence of Cu is unity. The silicates used in the studies by Ripley and Brophy (1995; intermediate data) and Schmitt et al. (1989; highest datum shown) contain percentage level of alkali elements (see Table 6). This suggests that the presence of alkali elements in iron-bearing silicates can cause changes in the formal valence of Cu (see text).

ies. Elliot et al. (1978) found that activity coefficients increase somewhat if MgO abundances are higher, but this effect is not as strong as the effect caused by lime or alumina additions.

4.3. Iron

The formal valences of iron in silicate melts vary from 1.24 ± 0.16 (Ruddle et al., 1966) to 2.88 ± 0.12 (Altman, 1978). Most values are around the expected theoretical valence of two for Fe^{2+}. The formal valence of 3.36 ± 0.28 for Fe from our S-free system is the highest valence in the set of data from Table 6 where comparison was possible. An analyses of the data in the literature shows that divalent iron is present in the silica-saturated iron silicates in the systems described in the literature (the iron data by Ruddle et al. 1966 scatter, and divalent Fe is likely to be present there too).

The experiments by Altman (1978) give a formal valence of 2.88, and the silicates contain ~8% CaO. This valence implies the presence of Fe^{2+} and Fe^{3+} and an increased Fe^{3+}/Fe^{2+} ratio in the silicate melt. Turkdogan (1983) describes in detail how lime additions increase Fe^{3+}/Fe^{2+} in iron silicate slags, which may be the reason for the observed effect in this subset of Altman's experiments. However, Holzheid and Palme (1996) used the same silicate compositions as we used here to determine the iron valence during metal/silicate partitioning under similar oxygen fugacities. They observed divalent iron. Thus increased CaO abundances cannot be the sole cause for the trivalent iron in our study and in that of Altman (1978). Above, we ascribed the presence of trivalent iron to redox

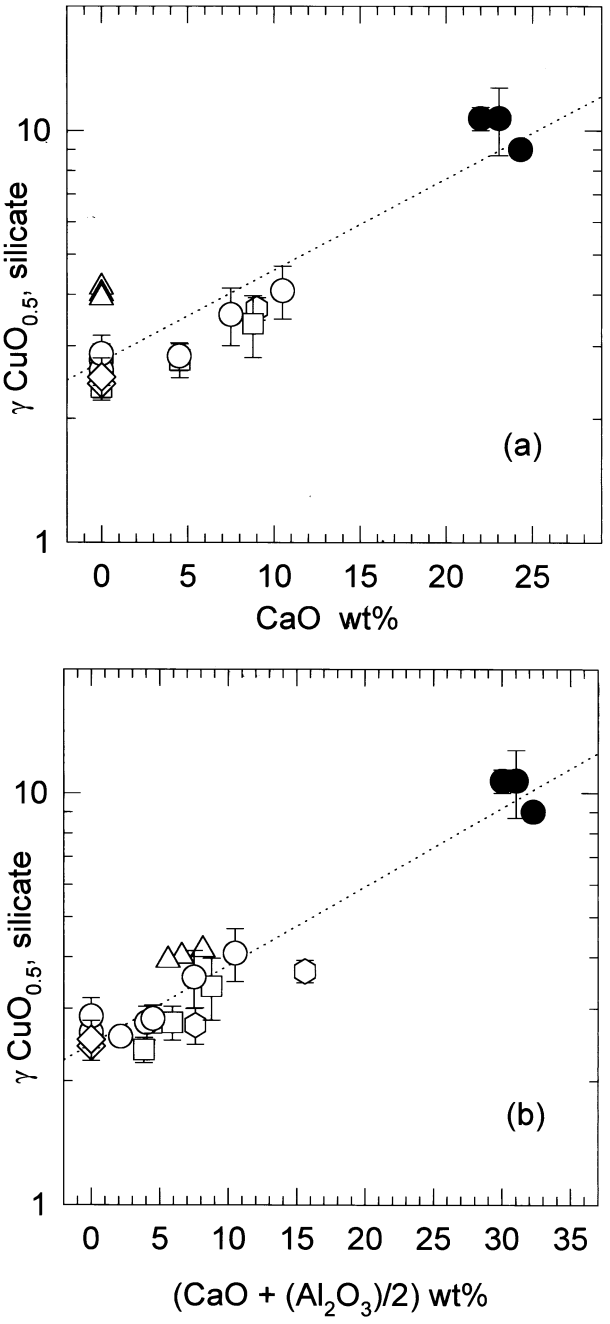

Fig. 5. Variation of the activity coefficients of $CuO_{0.5}$ in the silicate as function of CaO content (a) and CaO and Al_2O_3 content (b) of silicate melts at 1300°C. Closed circles: this work. Open circles: Elliot et al. (1978; silica-saturated Fe silicate). Hexagons: See and Rankin (1983; silica-undersaturated Fe silicate). Triangles: Reddy and Acholonu (1984; alumina-saturated Fe silicate). Squares: Altman (1978; silica-saturated iron silicate at ~1250°C). Diamonds: Ruddle et al. (1966; silica-saturated Fe silicates) and Taylor and Jeffes (1975; silica-saturated Fe silicates).

interactions with copper. Apparently the silicate melt must possess a certain basicity and contain abundant copper to increase the Fe^{3+}/Fe^{2+} ratio. Despite the large number of studies described in the literature, no further conclusions about the Fe valences affected by larger amounts of Cu in the system

are possible. This is another area where future experiments are needed.

The fit coefficients c_1 for iron metal/silicate partition coefficients in Table 6 show considerable variations of over 4 to 5 orders of magnitude. The smallest coefficient c_1 is obtained for silicate systems containing ferrous and ferric iron. We have seen above that the presence of large amounts of Cu may drive redox reactions toward Fe^{3+} in these particular systems. Therefore, the equilibrium constant embedded in c_1 (Eqn. 4c) for the exchange reaction of iron between metal and silicate is different than that for exchange reactions involving only Fe^{2+}. However, in systems where only Fe^{2+} is present, we have a unique equilibrium constant (no additional redox reactions) and the variation in c_1 shows the dependence of the iron oxide activity in the silicate melt as a function of melt composition (at constant temperature).

Systems containing Fe^{2+} were studied by Altman (1978) and Altman and Kellogg (1972), for which c_1 is about -7, and by Schmitt et al. (1989) and Holzheid and Palme (1996), for which c_1 is about -4.4 (Table 6). In these systems, the activity coefficients of iron oxide in the silicate and of Fe in the metal alloys are important. (There are also temperature variations among these studies, but temperature has only a small effect on c_1). At 1300°C, the activity coefficient of Fe in essentially pure Cu is 22.7 (Moser et al., 1985). Altman and Kellogg (1972) estimate an iron activity coefficient of 14.1 in their CuAu alloys for copper activities of 0.73. This activity coefficient also applies to iron in the CuAu alloys used by Altman (1978). The activity coefficients of Fe in the metal phases are about the same for all the systems containing copper. However, the activity coefficients of iron in the Fe-rich FeNi alloys used by Schmitt et al. (1989) and Holzheid and Palme (1996) are closer to unity. Eqn. 4c describes the dependence of c_1 on the activity coefficients in the alloy and silicate. A decrease of the activity coefficient of Fe in the metal alloy increases c_1. Therefore, the coefficient c_1 is expected to be about 1 log unit larger in systems that use FeNi alloys instead of Cu-rich CuFe alloys.

The remaining difference in c_1 between these studies must be due to changes in the iron oxide activity coefficient in silicate melts. The studies by Altman and Kellogg (1972) and Altman (1978) use silica-saturated iron oxide melts containing no or relatively small amounts of corundum, whereas the studies by Schmitt et al. (1989) and Holzheid and Palme (1996) used basaltic silicates with larger concentrations of CaO and Al_2O_3. However, this comparison assumes that the conversion factors from mass fractions to mole fractions are similar among all studies, which cannot be checked because these data are not given in the literature.

5. PARTITION COEFFICIENTS APPLICABLE TO PLANETARY DIFFERENTIATION

As mentioned above, partition coefficients for modeling planetary differentiation process are needed for Fe-rich FeNi alloys and relevant silicate compositions. The alloy compositions as well as the silicate compositions in the present study are clearly different (e.g., Cu metal instead of FeNi alloy). We transform our experimental equations for Cu metal/silicate and metal/sulfide partitioning to take into account the different activity coefficients of Cu in the FeNi alloy, sulfide, and silicate. To do so for metal/silicate partitioning, we substitute the activity coefficients of Cu in the metal and $CuO_{0.5}$ in the silicate from this study ("reference system") by the respective activity coefficients in the natural system (no superscript):

$$\log D^{met/sil}(Cu) = c_1^{ref} + \log \gamma^{ref}_{Cu,metal} - \log \gamma^{ref}_{CuO_{0.5},silicate} - \log \gamma_{Cu,metal} + \log \gamma_{CuO_{0.5},silicate} - 0.25 \log fO_2. \quad (25)$$

In Eqn. 25, the coefficient c_1 is reduced to $c_1^{ref} = -[\log K + \log(A/B)]$, i.e., the equilibrium constant for copper–copper oxide ($\log K = 0.847$) and the mole to mass fraction conversion factor ($\log (A/B) = 0.026$). The activity coefficients ($\gamma^{ref}_{Cu,\ metal} = 1$, $\gamma^{ref}_{CuO_{0.5}} = 10 \pm 1$) are determined above, and we obtain a generally applicable equation for the metal/silicate partition coefficient of Cu as function of oxygen fugacity at 1300°C:

$$\log D^{met/sil}(Cu) = -0.87(\pm 0.11) - \log \gamma_{Cu,metal} + \log \gamma_{CuO_{0.5},silicate} - 0.25 \log fO_2. \quad (26)$$

Only the respective activity coefficients of Cu in the metal and silicates are needed for modeling. The activity coefficient $\gamma_{CuO_{0.5},\ silicate}$ depends strongly on the silicate composition as seen in Figure 5b. We use the relation $\log \gamma_{CuO_{0.5},\ silicate} = 0.39 + 0.02 \cdot [CaO + Al_2O_3/2;\ wt\%]$ to describe the activity coefficient in silicate melt. Inserting into Eqn. 26 yields

$$\log D^{met/sil}(Cu) = -0.48 \pm (0.11) - \log \gamma_{Cu,\ metal} + 0.02 \cdot [CaO + Al_2O_3/2;\ wt\%] - 0.25 \log fO_2. \quad (27)$$

This equation applies to oxygen fugacities below $\log fO_2 = -9$ and systems that do not contain Cu as major constituent. As discussed above, redox reactions between Cu and Fe become important in systems containing percent levels of copper and iron at oxygen fugacities below $\log fO_2$ of approximately -11. Eqn. 27 may need an additional correction term for the oxygen fugacity if a dependence of the valence of Cu as a function of alkali content applies, as suggested from the comparison of data from the literature.

By analogy to Eqn. 25, we can write for the metal/sulfide partition coefficients

$$\log D^{met/sulf}(Cu) = c_1^{ref} + \log \gamma^{ref}_{Cu,metal} - \log \gamma^{ref}_{CuS_{0.5},sulfide} - \log \gamma_{Cu,metal} + \log \gamma_{CuS_{0.5},sulfide} - 0.25 \log fS_2. \quad (28)$$

In our experiments, essentially pure Cu and $CuS_{0.5}$ coexist, and the activity coefficients for the reference system are $\gamma^{ref}_{Cu,\ metal} = 1$ and $\gamma^{ref}_{CuS_{0.5},\ sulfide} = 1$. The coefficient c_1^{ref} incorporates the equilibrium constant and the log of the mole to mass fraction conversion factors (1.34 and 0.101, respectively). Inserting into Eqn. 28 gives the "generic" equation for metal/sulfide partitioning of Cu between Cu-bearing metal alloys and sulfides

$$\log D^{met/sulf}(Cu) = -1.24 - \log \gamma_{Cu,metal} + \log \gamma_{CuS_{0.5},sulfide} - 0.25 \log fS_2. \quad (29)$$

In natural systems, Cu partitions between metal, sulfide, and silicate, if all three phases coexist. This might be the case during core formation processes in the terrestrial planets and differentiated asteroids. Metal and sulfide phases are often assumed to form the cores, and therefore it is convenient to

write an equation for sulfide/silicate partitioning. Subtracting Eqn. 29 from Eqn. 27 gives

$$\log D^{sulf/sil}(Cu) = +0.76 - \log \gamma_{CuS_{0.5},sulfide} + 0.02 \cdot [CaO + Al_2O_3/2; wt\%] - 0.25 \log fO_2 + 0.25 \log fS_2. \quad (30)$$

The sulfur fugacity is controlled by the coexistence of iron metal and iron sulfide, if metal and sulfide are present. Eqn. 30 simplifies further by substituting the sulfur fugacity by $-2 \cdot \log K_{FeS}$. By use of a value of 2.127 for $\log K_{FeS}$ (Chase, 1998), we obtain

$$\log D^{sulf/sil}(Cu) = -0.30 - \log \gamma_{CuS_{0.5},sulfide} + 0.02 \cdot [CaO + Al_2O_3/2; wt\%] - 0.25 \log fO_2. \quad (31)$$

We close this section by applying Eqns. 27 and 31 to partitioning of Cu in the Earth and Mars. Iron-rich FeNi alloys are involved in core formation in the terrestrial planets. In FeCu alloys with infinitely small amounts of Cu $\gamma_{Cu,\ metal} = 9.18$ at 1300°C (Moser et al., 1985). The activity coefficient of $CuS_{0.5}$ in FeS calculated from the Temkin model (see Bale and Toguri, 1976) is $\gamma_{CuS_{0.5}sulfide} = 0.998$ for $X_{CuS_{0.5}} \leq 0.01$. Therefore, the activity coefficient of $CuS_{0.5}$ in FeS is taken as unity here. We use the bulk silicate compositions for Earth and Mars (Lodders and Fegley, 1998) to find the amount of CaO and Al_2O_3 in the silicate. The metal/silicate partition coefficients for Cu then become

$$\log D^{met/sil}(Cu, \text{“Earth”}) = -1.33 - 0.25 \log fO_2 \quad (32a)$$

and

$$\log D^{met/sil}(Cu, \text{“Mars”}) = -1.37 - 0.25 \log fO_2. \quad (32b)$$

The small difference in the bulk silicate compositions of Earth and Mars leads to a small decrease in the partition coefficients for Mars at constant oxygen fugacity. However, if silicate compositions change during planetary differentiation, the partition behavior of Cu is affected. For example, crust formation decreases CaO and Al_2O_3 concentrations in the residual silicate mantle. In that case, Cu dissolution is more favorable in the mantle, and partitioning of Cu into the core is less efficient (smaller metal/silicate partition coefficient).

The sulfide/silicate partition coefficients for Earth and Mars (for fS_2 buffered by Fe-FeS) from Eqn. 31 are

$$\log D^{met/sil}(Cu, \text{“Earth”}) = -1.19 - 0.25 \log fO_2 \quad (32a)$$

and

$$\log D^{sulf/sil}(Cu, \text{“Mars”}) = -0.22 - 0.25 \log fO_2. \quad (32b)$$

The Cu sulfide/silicate partition coefficients are about 10 times larger than the corresponding metal/silicate partition coefficients, independent of oxygen fugacity (Eqns. 32a, 33a, and 32b and 33b, respectively). This shows that copper is more chalcophile than siderophile.

We now use the partition coefficients to test whether or not the observed silicate abundances of Cu in the Earth and Mars are consistent with chemical equilibrium between core-forming metal and sulfide and the silicate protomantle. The concentration of Cu in the silicate portion (c_{sil}) is derived from the mass-balance equation relating partition coefficients, mass fractions (W) of silicate, sulfide, and metal in the planet, and the total abundance of Cu (c_{tot}) in the planet

$$C_{sil} = c_{tot} \cdot [W_{sil} + D^{met/sil} \cdot W_{met} + D^{sulf/sil} \cdot W_{sulf}]^{-1}. \quad (34)$$

The total planetary Cu abundance is obtained from the CI-chondritic Cu/Mg ratio and the Mg abundance in the planetary silicate portion. The mass fractions of silicate, sulfide, and metal for Mars are taken as 0.794, 0.06, 0.146 (Lodders and Fegley, 1997, and references therein). We adopt an oxygen fugacity range of IW-0.5 to IW-1 for Mars and calculate Cu abundances of 6.3 to 8.3 ppm in the silicate. These abundances are close to the Cu abundances of 2.9 to 5.5 ppm obtained independently from element correlations, supporting earlier conclusions of metal–silicate (i.e., core-mantle) equilibrium for Mars (e.g., Wänke and Dreibus, 1994). The Martian core must contain large amounts of sulfide. Extraction of Cu from the silicate by sulfide is necessary because the metal/silicate partition coefficients at the adopted oxygen fugacities are too small to account for the observed Cu abundance.

We apply the same calculation to Earth using mass fractions of 0.675 (silicate), 0.025 (sulfide), and 0.30 (metal) (see Lodders and Fegley, 1998). We use an oxygen fugacity of IW-2.3, which is required for equilibration of a metallic core with ~8% FeO in the bulk silicate Earth (Holzheid and Palme, 1996; O'Neill and Palme, 1998). We calculate 5 ppm Cu for the bulk silicate Earth, which is too small when compared to independently derived Cu abundances of ~30 ppm (see Lodders and Fegley, 1998, pp. 135–139). If no sulfide is involved in metal–silicate equilibrium, the calculated Cu abundance in the silicate is 10 ppm. Thus the observed Cu abundance in the Earth's silicates is too high to be explained by metal–silicate equilibrium at moderate pressures and temperatures.

Volatility depletions may also play a role in determining the Cu abundance in the Earth's mantle. Othani et al. (1995, 1997) discuss that Cu may have been depleted in the planetesimals accreting to Earth. In this scenario the assumption of CI abundances in Eqn. 34 is not justified. Ohtani et al. (1995, 1997) suggest a volatility depletion factor of 0.25 to 0.6 for Cu. In that case, calculated abundances from metal–sulfide/silicate partitioning are even lower.

So far, we have not considered pressure effects on the metal–metal sulfide–silicate partitioning. Metal–silicate equilibration responsible for the observed siderophile element pattern in the Earth's mantle may have occurred during metal segregation from the base of a deep magma ocean. Li and Agee (1996, 1997), Ohtani et al. (1995, 1997), and Righter and Drake (1997, 2000) investigated metal/silicate partitioning for a suite of elements under elevated pressures and temperatures to test this hypothesis. The Cu metal/silicate partition coefficients are less than unity at ~25 GPa and ~2000 K assumed for the base of such a magma ocean (Ohtani et al., 1995; Righter and Drake, 2000). Under these conditions, the extraction of Cu from the silicate is less efficient and more Cu should reside in the silicates than observed. To adjust the Cu abundances to observed levels, Ohtani et al. (1995, 1997) invoke depletion of Cu by volatility, which is also discussed by Li and Agee (1997) and Righter and Drake (2000).

It is already well known (e.g., Schmitt et al., 1989; Holzheid and Palme, 1996) that the observed abundances of Cu and other

moderately siderophile elements in the Earth's mantle are incompatible with metal–silicate equilibrium under moderate temperatures and pressures. Ringwood (1984) and Wänke et al. (1984) proposed that the Earth accreted heterogeneously with successive changes in oxidation state from highly reducing to oxidizing conditions. The reducing conditions are necessary to account for the mass of the metallic core, whereas the more oxidizing conditions are required to account for the final oxidation state (FeO content) of the mantle. O'Neill and Palme (1998) discuss how the siderophile element abundances (including Cu) of the Earth's mantle reflect heterogeneous accretion.

We favor the view that metal and silicate equilibrated under low pressures and temperatures in the top layer of the growing planet where high-pressure effects may not play a major role. The Earth (and other rocky planets) grew by accumulation of small undifferentiated and/or differentiated planetesimals. As described by Stevenson (1990), the dispersed metal and metal sulfide from an incoming undifferentiated (chondrite-like) planetesimal first equilibrates with surrounding silicate of the protomantle under low pressure. Equilibration with the silicate stops when the metallic melt agglomerates to larger melt pools that rapidly sink to the growing core. If the incoming planetesimals were differentiated, their metal–silicate equilibration happened under low total pressures. The core or cores of such accumulating planetesimals combine with the Earth's protocore without equilibrating with the silicate because density separation may not allow a long residence time of such cores in the protomantle. The mantle of the Earth would only inherit the Cu content from the silicates of the accreting differentiated planetesimals. If equilibration of silicates and metal in the planetesimals occurred at higher oxygen fugacities, their silicates contribute more Cu to the Earth's mantle. Accretion of more oxidizing undifferentiated material to the Earth has the same effect, because then partition coefficients of Cu are smaller and less Cu is removed by metal–sulfide into the core.

In conclusion, the calculated Cu abundance in the bulk silicate Earth from low pressure and temperature partition coefficients is lower than observed (assuming metal–silicate equilibration at constant fO_2). This points towards heterogeneous accretion for the Earth. On the other hand, high pressure and temperature partitioning result in higher Cu abundances than observed and additional volatility depletions of Cu must be invoked. We prefer the heterogeneous accretion model for the Earth, which is supported by several different arguments (see O'Neill and Palme 1998 for detailed discussion). Given the arguments above, we think that metal–silicate equilibration responsible for the observed siderophile element abundances occurred at low pressures and temperatures. Such low pressure and temperature partition coefficients can explain the Cu abundance for Mars. Still, future work is needed to quantitatively model the siderophile element distribution in the heterogeneously accreting Earth.

6. CONCLUSION

Partitioning of copper was investigated between silicate liquids and liquid copper (and CuFe alloys) at 1300°C as a function of silicate composition and oxygen and sulfur fugacities in four different systems (Fe- and S-free; Fe-free and S-bearing; Fe-bearing and S-free; and Fe- and S-bearing). At oxygen fugacities above 10^{-11} bar, monovalent copper is dissolved in silicates saturated with Cu metal or Cu-rich CuFe alloys, independent of whether sulfur and iron are present or absent. At oxygen fugacities $<10^{-11}$ bar, the formal valence of Cu decreases when iron is present in the silicates, which we explain by redox equilibria between copper and iron. We find no evidence of sulfidic dissolution of Cu in the silicate. Sulfidic dissolution of Fe in the silicate seems to occur because silicate iron abundances are higher in sulfur-bearing experiments than sulfur-free ones. However, sulfur concentrations in these silicates are lower than expected from FeS dissolution because sulfur is removed from the silicate by oxide/sulfide exchange reactions involving Cu.

Increasing the temperature from 1300° to 1514°C increases the Cu solubility (decreases the metal/silicate partition coefficient) at an oxygen fugacity 0.5 log units below the IW buffer in S-free systems. The metal–silicate partition coefficients of Cu do not decrease linearly with 1/T as theoretically expected because the silicate melt was enriched in Al_2O_3 by reactions with the corundum crucibles used, which causes an increase in Cu metal/silicate partitioning. A comparison with literature data shows that Cu partition coefficients increase with increasing CaO and Al_2O_3 content of silicate melts under otherwise constant conditions (temperature, oxygen fugacity). This implies that the activity coefficient of $CuO_{0.5}$ increases with CaO and Al_2O_3 content of the silicate. We derive an activity coefficient $\gamma_{CuO_{0.5}} = 10 \pm 1$ in the MgO-rich basaltic silicates used here.

The comparison with literature data suggests that the simultaneous presence of alkali elements and iron oxides causes an apparent increase in the Cu valence. This is a topic that needs further investigation.

The derived metal/silicate and metal/sulfide partition coefficients are applied to planetary core formation in the Earth and Mars. The observed Cu abundances in the Earth's silicates cannot be easily explained by simple metal/silicate equilibrium at low pressures and temperatures and point towards heterogeneous accretion. The observed Cu abundances for Mars are consistent with low pressure and temperature equilibrium between silicate and a sulfur-rich core.

Acknowledgments—The experiments were carried out during 4 months' stay of A. Holzheid at the Planetary Chemistry Laboratory at Washington University in St. Louis. We thank Bruce Fegley for advice and fruitful discussions. We thank D. Kremser, Washington University, St. Louis, and D. Krauβe, Bayerisches Geoinstitut, Bayreuth, for help and assistance in analyzing the samples by electron microprobe. Financial support was provided through a 4 months exchange scholarship of the German Academic Exchange Service to one of us (A. Holzheid). The experiments were partially supported by a grant from the NASA Origins Program. The McDonnell Center for the Space Sciences provided support for publication of the color figure. Comments by associate editor C. Romano, referee H. Keppler, and two anonymous referees are appreciated.

Associate editor: C. Romano

REFERENCES

Ajersch F. and Toguri J. M. (1969) Diffusion of copper in liquid fayalite slags. *Can. Met. Q.* **9,** 507–511.

Altman R. (1978) Influence of Al_2O_3 and CaO on solubility of copper in silica-saturated iron silicate slag. *Trans. Inst. Min. Metall.* **87,** C23–C28.

Altman R. and Kellogg H. H. (1972) Solubility of copper in silica-saturated iron silicate slag. *Trans. Inst. Min. Metall.* **81,** C163–C175.

Armstrong J. T. (1988) Quantitative analysis of silicate and oxide minerals: Comparison of Monte-Carlo, ZAF and Phi-Rho-Z procedures. Microbeam Analysis–1988 (ed. D. E. Newbury) pp. 239–246 San Francisco Press.

Bale C. W. and Toguri J. M. (1976) Thermodynamics of the Cu-S, Fe-S and Cu-Fe-S systems. *Can. Metall. Q.* **15,** 305–318.

Borisov A., Palme H., and Spettel B. (1994) Solubility of palladium in silicate melts: Implications for core formation in the Earth. *Geochim. Cosmochim. Acta* **58,** 705–716.

Chase M. W. (1998) *NIST-JANAF Thermochemical Tables*, 4th ed. American Institute of Physics.

Dietzel A. (1945) Über das Anlaufen der durch Metallkolloide gefärbten Gläser. Z. *Elektrochem.* Zeitschrift für Elektrochemie **51,** 32–37.

Elliot B. J., See J. B., and Rankin W. J. (1978) Effects of slag composition on copper losses to silica saturated iron silicate slags. *Trans. Met. Min. Met.* **87,** C204–C211.

Gurvich L. V., Veyts I. V., and Alcock C. B. (1989) *Thermodynamic Properties of Individual Substances*, Vols. 1–4, 4th ed. Hemisphere.

Hofmeister A. and Rossman G. R. (1985) Exsolution of metallic copper from Lake County labradorite. *Geology* **13,** 644–647.

Holzheid A. and Palme H. (1996) The influence of FeO on the solubilities of cobalt and nickel in silicate melts. *Geochim. Cosmochim. Acta* **60,** 1181–1193.

Holzheid A., Palme H., and Chakraborty S. (1997) The activities of NiO, CoO and FeO in silicate melts. *Chem. Geol.* **139,** 21–38.

Johnston W.D and Chelko A. (1966) Oxidation-reduction equilibria in molten $Na_2O \cdot 2SiO_2$ glass in contact with metallic copper and silver. *J. Am. Cream. Soc.* **49,** 562–564.

Li J. and Agee C. B. (1996) Geochemistry of mantle-core differentiation at high pressure. *Nature* **381,** 686–689.

Li J. and Agee C. B. (1997) Partitioning of volatile elements during core-mantle differentiation (abstract 1666). In *Lunar and Planetary Science XXVIII*. Lunar and Planetary Institute (CD-ROM).

Lodders K. and Palme H. (1991) The role of sulfur in planetary core formation. *Meteoritics* **26,** A366.

Lodders K. and Fegley B. (1997) An oxygen isotope model for the composition of Mars. *Icarus* **126,** 373–394.

Lodders K. and Fegley B. (1998) *The Planetary Scientist's Companion.* Oxford University Press.

Maruyama N. and Ban-ya S. (1980) Measurements of activities in liquid Fe-Cu, Fe-Cr and Fe-Sn alloys by a transportation method. *J. Jpn. Inst. Metals* **44,** 1422–1431.

Moser Z., Zakulski W., Spencer P., and Hack K. (1985) Thermodynamic investigations of solid Cu-Ni and Fe-Ni alloys and calculations of the solid state miscibility gap in the Cu-Fe-Ni system. *CALPHAD* **9,** 257–269.

Nagamori M. (1974) Metal loss to slag: Part I. Sulfidic and oxidic dissolution of copper in fayalite slag from low grade matte. *Met. Trans.* **5,** 531–538.

O'Neill H. St. C. and Palme H. (1998) Composition of the silicate Earth: Implications for accretion and core formation. In *The Earth's Mantle: Structure, Composition and Evolution* (ed. I. Jackson), pp. 3–126. Cambridge University Press.

Ohtani E., Yurimoto H. Segawa T., and Kato T. (1995) Element partitioning between $MgSiO_3$ perovskite, magma, and molten iron: Constraints for the earliest processes of the Earth–Moon system. In *The Earth's Central Part: Its Structure and Dynamics* (ed. T. Yukutake), pp. 287–300. Terra Scientific.

Ohtani E., Yurimoto H., and Seto S. (1997) Element partitioning between metallic liquid, silicate liquid, and lower-mantle minerals: Implications for core formation in the Earth. *Phys. Earth Planet. Int.* **100,** 97–114.

Pouchou J. L. and Pichoir F. (1984) A new model for quantitative X-ray microanalysis. Part I: Application to the analysis of homogeneous samples. *Recherche Aérospatiale* **3,** 13–38.

Rajamani V. and Naldrett A. J. (1978) Partitioning of Fe, Co, Ni, and Cu between sulfide liquid and basaltic melts and the composition of Ni-Cu sulfide deposits. *Econ. Geol.* **73,** 82–93.

Reddy R. G. and Acholonu C. C. (1984) Activity coefficient of $CuO_{0.5}$ in alumina saturated iron silicate slags. *Met. Trans.* **15B,** 345–349.

Richardson F. D. and Billington J. C. (1956) Copper and silver in silicate slags. *Trans. Inst. Min. Metal.* **65,** 273–297.

Righter K. and Drake M. J. (1997) Metal–silicate equilibrium in a homogeneously accreting earth: New results for Re. *Earth Planet. Sci Lett.* **146,** 541–553.

Righter K. and Drake M. J. (2000) Metal/silicate equilibrium in the early Earth—New constraints from the volatile moderately siderophile elements Ga, Cu, P, and Sn. *Geochim. Cosmochim. Acta* **64,** 3581–3597.

Ringwood A. E. (1984) The Earth's core: Its composition, formation and bearing upon the origin of the earth. *Proc. R. Soc. Lond. A* **395,** 1–46.

Ripley E. M. and Brophy J. G. (1995) Solubility of copper in a sulfur-free mafic melt. *Geochim. Cosmochim. Acta* **59,** 5027–5030.

Ruddle R. W., Taylor B., and Bates A. P. (1966) The solubility of copper in iron silicate slags. *Trans. Inst. Min. Metall.* **75,** C1–C12.

Schmitt W., Palme H., and Wänke H. (1989) Experimental determination of metal/silicate partition coefficients for P, Co, Ni, Cu, Ga, Ge, Mo, and W and some implications for the early evolution of the Earth. *Geochim. Cosmochim. Acta* **53,** 173–185.

Schreiber H. D., Schreiber C. W., and Kozak S. J. (1992) Novel formulations of amber glass. *Am. Ceram. Soc. Bull.* **71,** 1829–1835.

See J. B. and Rankin W. J. (1983) Effect of Al_2O_3 and CaO on solubility of copper in silica–unsaturated iron silicate slags at 1300°C. *Trans. Inst. Min. Metall.* **92,** C9–C13.

Stevenson D. J. (1990) Fluid dynamics of core formation. In *Origin of the Earth* (eds. H. E. Newsom and J. H. Jones), pp. 231–249. Oxford University Press.

Taylor J. R. and Jeffes J. H. E. (1975) Activity of cuprous oxide in iron silicate of various compositions. *Trans. Inst. Min. Metall.* **84,** C18–C24.

Toguri J. M. and Santander N. H. (1969) The solubility of copper in fayalite slags at 1300°C. *Can. Metall. Q.* **8,** 167–174.

Toguri J. M. and Santander N. H. (1972) Distribution of copper between Cu-Au alloys and silica saturated fayalite slags. *Met. Trans.* **3,** 586–588.

Turkdogan E. T. (1983) *Physicochemical Properties of Molten Slags and Glasses.* Metals Society.

Wänke H., Dreibus G., and Jagoutz E. (1984) Mantle chemistry and accretion history of the Earth. In *Archean Geochemistry* (ed. A. Kröner), pp. 1–24. Springer Verlag.

Wänke H. and Dreibus G. (1994) Chemistry and accretion history of Mars. *Phil. Trans. R. Soc. Lond.* **A349,** 285–293.

Weyl W. A. (1954) *Coloured Glasses.* Society of Glass Technology.

Winther K. T., Watson E. B., and Korenowski G. M. (1998) Magmatic sulfur compounds and sulfur diffusion in albite melt at 1 GPa and 1300–1500°C. *Am. Min.* **83,** 1141–1151.